CHAPTER - 3

Synthesis and study of symmetrical dicyano derivative of oxa[7]helicene

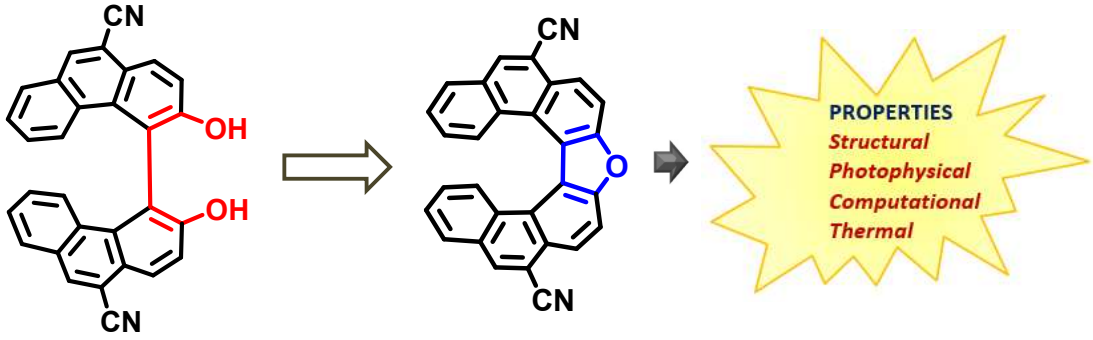

Table of Contents

3.1 Introduction to Oxahelicenes

Incorporating heteroatoms into the helical backbone modifies the electronic structure and overall physical properties. Heterohelicenes consisting of oxygen atom as a part of ring system are known as oxahelicenes. The chemistry of oxa[*n*]helicene and the derivatives have gained much attention due to their other applications. The presence of oxygen containing rings in the framework of such compounds is expected to show high HOMO levels[1] and have found applications in electronic devices such as organic light emitting diodes and organic field-effect transistors.[2] Moreover, the synthetic methods to incorporate furan ring into a helicene scaffold has not been much explored.

One of the most convenient methods to build furan ring in a helical skeleton includes the use of BINOL based systems. Carolina and co-workers reported the synthesis of 7-oxa-[5]helicene-3,11-dicarboxylic acid from rac-6,6'-dibromo-1,1'-binaphthol, where the yield was poor and hence, difficult to scale-up.[3] Thongpanchang and co-workers reported the first large-scale synthesis of oxa[5]helicene derivatives by C-C homo coupling of 2,7-dihydroxynaphthalene, followed by dehydration. However, these oxa[5]helicene derivatives **4** were found to be planar and achiral (**Scheme 3.1**).[4]

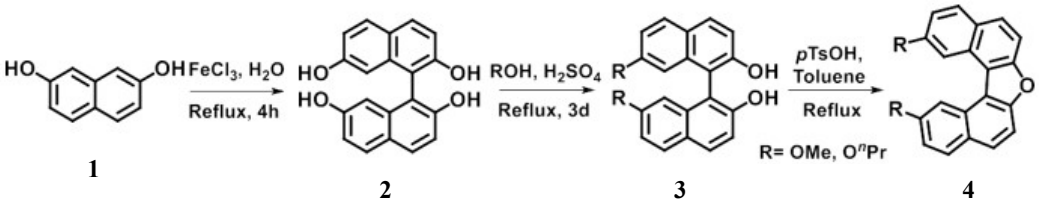

Scheme 3.1: Synthesis of 2,12-disubstituted-oxa[5]helicenes

A similar strategy was used by Dotz and coworkers to synthesize a series of oxa[5]helicenes. Here, the furan ring was constructed by activation of one of the –OH groups of the BINOL derivative **5**, followed by intramolecular cyclization to form substituted [5]helicene **7** (**Scheme 3.2**). Later, it was subjected to chromium-templated benzannulation with different alkynes to obtain the higher members of helical mono- and bis-quinone oxahelicenes **10** (**Scheme 3.3**).[5]

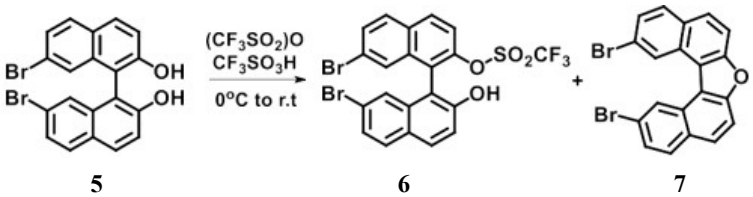

Scheme 3.2: Synthesis of 2,12-dibromo-oxa[5]helicene

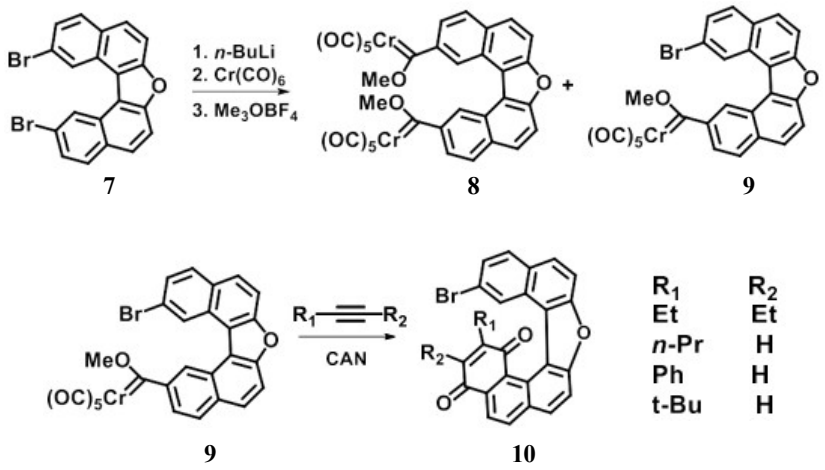

7 8 9 9 10

***Scheme 3.3**: Synthesis of oxahelicene quinones*

The single crystal X-ray analysis of 2-hydroxy-7-oxa[5]helicene **13** revealed a relatively flat structure of the oxa[5]helicene unit which indicates that the helical enantiomers have low configurational stability at room temperature. However, by increasing the steric crowding with the introduction of nitro group at 1-position of oxa[5]helicene **14**, ^{1}H NMR (at -20 °C) of **15** exhibited the presence of two helical isomers at low temperature (**Scheme 3.4**).[6]

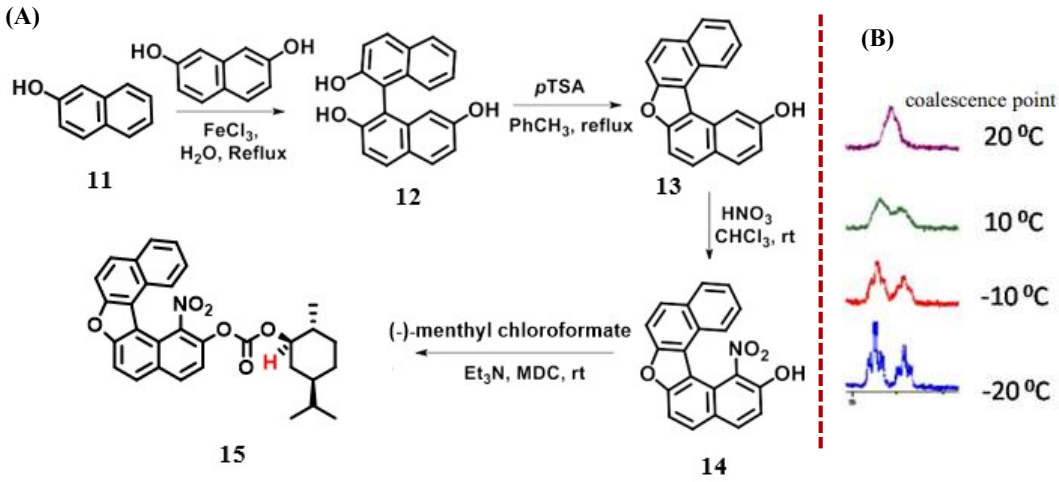

11 12 13 14 15

***Scheme 3.4**: (a) Synthesis of 1-nitro-2-hydroxy-7-oxa[5]helicene and its menthyl carbonate (b) VT NMR showing the signal for proton at chiral center (marked in red)*

As the resolution of 1-substituted oxa[5]helicenes was difficult due to their rapid racemization at room temperature, focus was shifted towards the synthesis and study of higher analogues of oxahelicenes. The synthesis of dioxa[6]helicene **19**, an analogue of oxa[5]helicene containing an additional furan ring was reported by Bechgaad and co-workers (**Scheme 3.5**).[7]

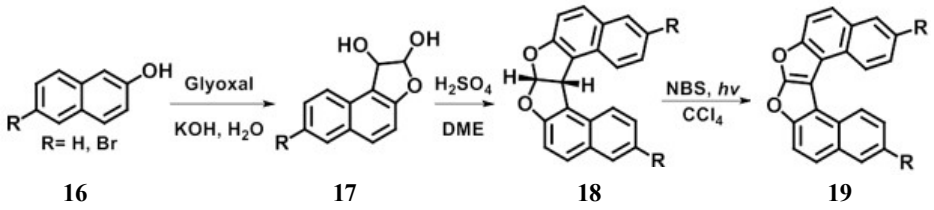

***Scheme 3.5**: Synthesis of dioxa[6]helicene*

This strategy directed the synthesis of many derivatives of dioxa[6]helicene. Karnik and co-workers reported the synthesis of dioxa[6]helicene diol **23**, by using a slightly modified method. Dioxa[6]helicene diol **23** was resolved by forming diastereomers with (1*S*)-camphor sulfonyl chloride (**Scheme 3.6**). The optically pure dioxa[6]helicene diol was used in the recognition of trans-1,2- cyclohexanediamine as a sensor.[8]

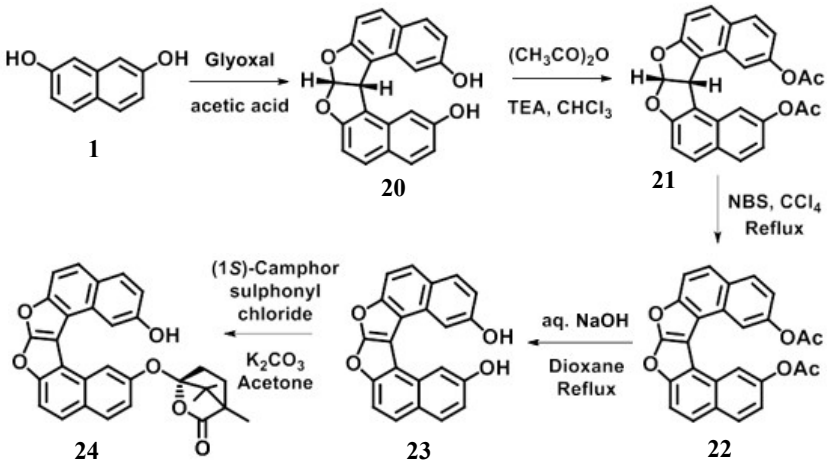

***Scheme 3.6**: Synthesis of dioxa[6]helicene diol*

Later they used dihyrodioxa[6]helicene diol to prepare a C*s*-symmetric rigid organophosphoric acid **26** (**Scheme 3.7**) which was further utilized as a chiral system in the determination of absolute configuration of some 1,2-amino alcohols by induced CD studies.[9]

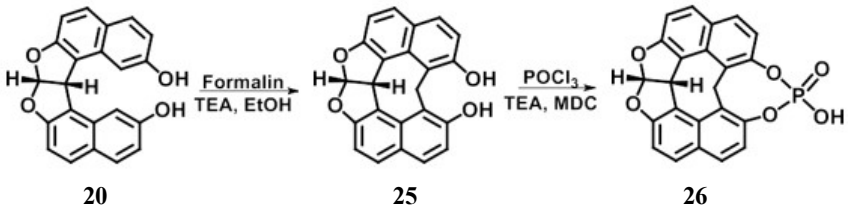

***Scheme 3.7**: Synthesis of phosphoric acids derived from dihyrodioxa[6]helicene*

Rodriguez, Bonne and co-workers reported the synthesis of configurationally stable dioxa[6]helicene **30** by using simple achiral precursors. The helicity was generated and controlled by an organocatalyzed domino Michael/C−O alkylation step, which afforded 2-nitrodihydrofuran containing two stereogenic carbon atoms as well as helical shape. This was followed by an eliminative aromatization to obtain dioxa[6]helicene **30** (**Scheme 3.8**).[10]

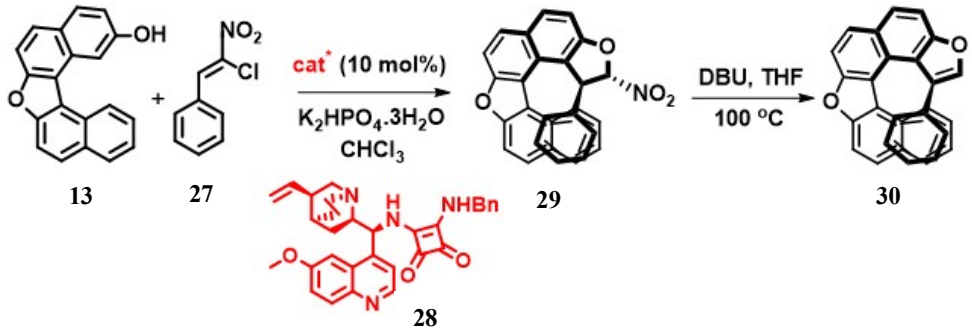

***Scheme 3.8**: Synthesis of configurationally stable dioxa[6]helicene 30*

The synthesis of 5- and 6- membered oxahelicenes was easy compared to the higher membered analogues. Synthesis of dioxa[7]helicene **35** containing two naphthafuran units *ortho*-fused to a central benzene ring, was reported by using oxidative tandem cyclization of the bis-2-naphthol linked by an *o*-phenylene group (**Scheme 3.9**). **35** was resolved by the help of chiral HPLC but was found to isomerize at ambient temperatures.[11]

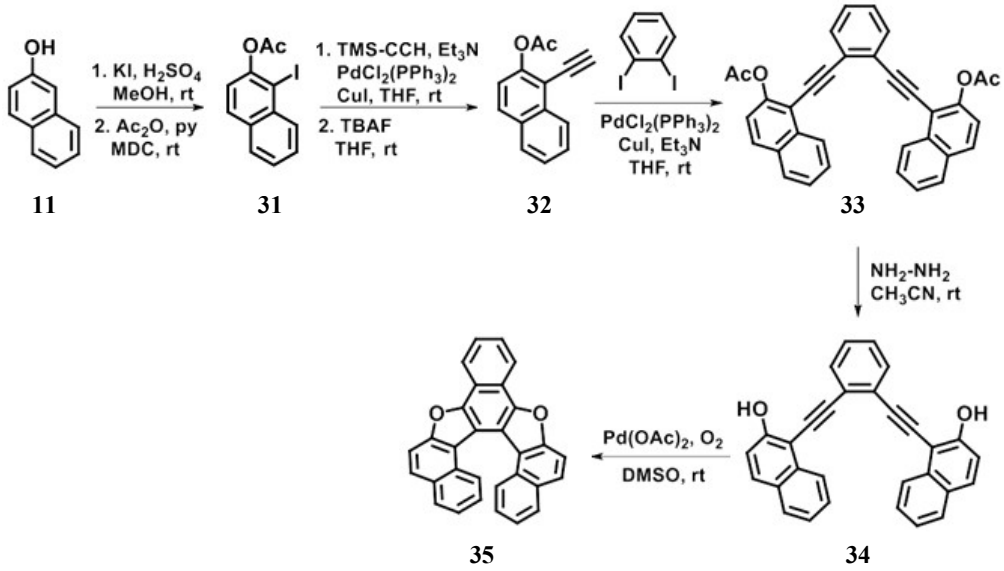

***Scheme 3.9**: Synthesis of dioxa[7]helicene 35*

Looking at an unsuccessful resolution of dioxa[7]helicene **35**, an oxa[7]helicene, containing a single furan ring in the helical skeleton was synthesized. Nozaki and co-workers used a similar strategy to the one used by Thongpanchang group (for the synthesis of oxa[5]helicenes) using different analogues of BINOL and their derivatives. Here, a Pd-catalysed intramolecular *O*-arylation of mono triflates or nonaflates was employed to afford oxa[7]helicene with excellent yield (**Scheme 3.10**).[12] The oxahelicenes were obtained in optically active forms as the biaryl intermediate was successfully resolved by using (1*S*)-camphor sulfonyl chloride. However, it was racemized at 100 °C.

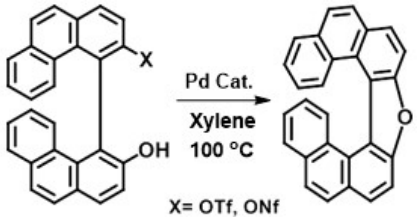

36 **37**

***Scheme 3.10**: Synthesis of oxa[7]helicene*

In this synthetic stategy, the C-C oxidative coupling step of naphthols and its analogues often generates helical quinones as by-product, lowering the yield of the desired helicene. Salim and co-workers synthesized a oxa[9]helicene **40**. They utilized the helical quinones to obtain the corresponding oxahelicene by treating it with Lawesson's reagent or phosphorus pentasulfide (**Scheme 3.11**).[13]

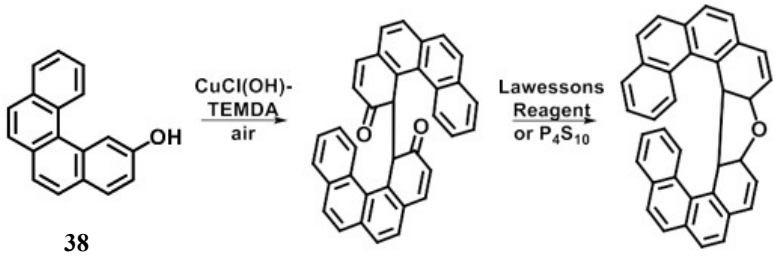

38 **39** **40**

***Scheme 3.11**: Synthesis of oxa[9]helicene*

These oxa[9]helicene derivatives were successfully resolved by chiral HPLC.[13c] Other derivatives of oxa[9]helicenes namely 11-oxa[9]helicene and 9- diethyleneglycoxy-11-oxa[9]helicene were synthesized by this strategy and were used in the preparation of thin monolayered films with the help of Langmuir technique.[14]

Another higher analogue of oxahelicene, a 7,12,17-trioxa[11]helicene **42** was synthesized by a series of oxidative coupling followed by dehydrative cyclization reaction (**Scheme 3.12**). The helicene **42** was characterized by single-crystal X-ray analysis and photochemical studies which showed interesting properties.[15]

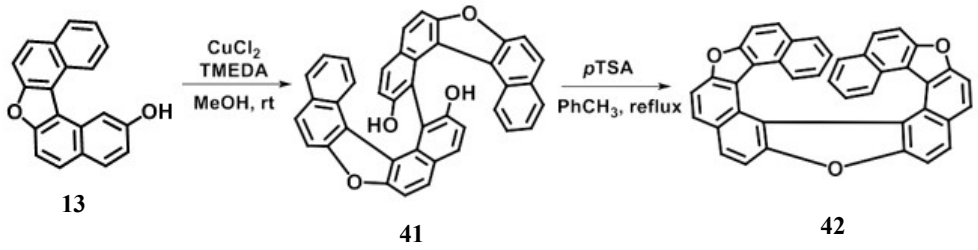

Scheme 3.12: Synthesis of trioxa[11]helicene

Recently, Yorimitsu and co-workers reported the synthesis of dioxa[8]helicene in enantiomerically enriched form. A cascade of Pummerer reaction/ sigmatropic rearrangement was employed to afford the highly crowded ternaphthyl intermediate **44**. This intermediate was resolved using optically active camphor sulphonyl chloride and the subsequent cyclization under basic conditions afforded the helicene **45** in good enantiomeric excess (**Scheme 3.13**).[16]

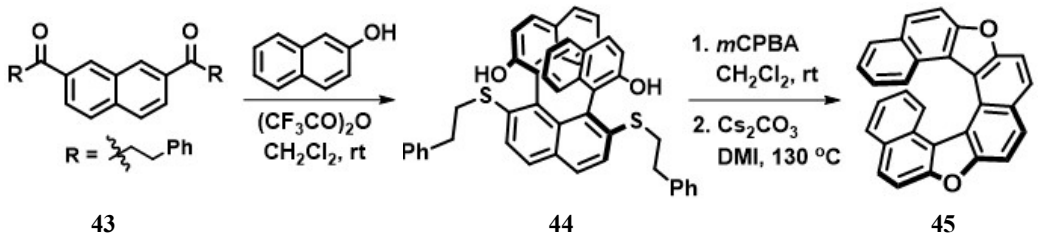

Scheme 3.13: Synthesis of dioxa[8]helicene

3.2 Cyano helicenes and spontaneous resolution

The favorable supramolecular interactions between the molecules of same chiral description, may lead to isolation of the crystals with enriched enantiomers resulting in the spontaneous resolution. For the success of this unusual phenomenon of spontaneous resolution, presence of suitable substituents in the helical backbone is necessary. Literature shows very few synthons having the ability to show spontaneous resolution. Wachsmann and co-workers synthesized seven derivatives of hexahelicenes, out of which only the cyano hexahelicene **46** showed spontaneous resolution[17] (**Figure 3.1**). The crystal structure of **46** revealed that the

presence of intermolecular π-π interactions were responsible for such phenomenon. Separation of isomers of 6,13-dicyano[7]helicene **47** by the 2D spontaneous resolution on the surface of Cu(111) is another such example.[18] Here, the self-association was based on CN···HC(Ar) hydrogen bonding and dipolar CN···CN interactions (**Figure 3.1**).

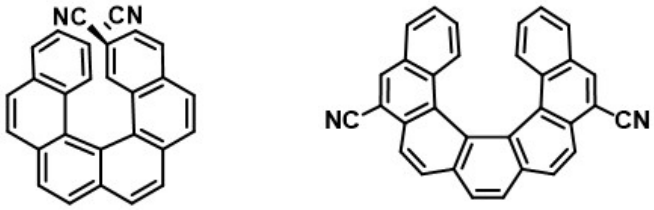

46 **47**

***Figure 3.1**: Reported cyano helicenes showing spontaneous resolution*

The separation of crystals of the enriched isomers of 5,13-dicyano-9-butyl-9*H*-aza[7]helicene **49** was achieved by our group by crystallization from 1,2-dichloroethane.[19] In addition to **49**, several other derivatives of dicyano aza[7]helicene were investigated, but none of them resulted in spontaneous resolution. The detailed study of supramolecular interactions gave us some insight in the correlation of structure and favorable intermolecular interactions resulting in such separation. Its oxygen analogue, 5,13-dicyano-9-oxa[7]helicene **48** was also synthesized by our group. This molecule too could not result in its spontaneous resolution. The crystallization study was severely hampered by its very poor solubility in most of the common organic solvents.[20] In this chapter we present our efforts to synthesize the isomer **50** where the cyano groups are attached at different positions (**Figure 3.2**).

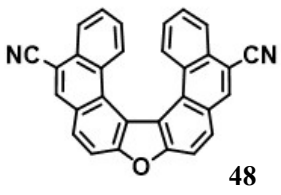

48

Eur. J. Org. Chem. **2018**
Spontaneous resolution was not observed

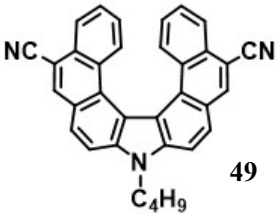

49

Cryst. Growth Des. **2019**
Spontaneous resolution was observed

50

Target molecule

***Figure 3.2**: Cyano helicenes reported by Bedekar group*

In the previous study of the spontaneous resolution of **49**, a key supramolecular interaction, H-bonding, was observed between the nitrogen of cyano group of one molecule and the C-H *ortho* hydrogen of other molecule, for spontaneous resolution between the enantiomers of the same description. This depended on the precise electronic nature of the hydrogen for

successful chiral recognition between the two molecules of some optical description. In an effort to extrapolate this hypothesis we designed molecule **50** and attempted its synthesis and crystallization study. It is assumed that by changing the location of the cyano groups with respect to the oxygen of the oxa[7]helicene framework, we can anticipate some variation in the electropositive nature of hydrogen atoms at C-5 and C-13 which may influence its physical characteristics.

3.3 Results and Discussion

3.3.1 Synthesis of 6,12-dicyano-9-oxa[7]helicene

The retrosynthetic scheme was designed such that the furan moiety was introduced in the last step (**Figure 3.3**). The synthesis of the target molecule could be achieved *via* cyclodehydration of the corresponding bis-phenanthrol, a BINOL analogue. This bis-phenanthrol can be obtained from C-C oxidative homocoupling of the corresponding phenanthrol derivative. As it is easy to synthesize phenanthrene motifs on a multi-gram scale, this retrosynthetic path proved to be ideal for the synthesis of such target molecule. The photochemical oxidative cyclization method was used for the synthesis of phenanthrene derivative, as the precursor stilbene can be synthesized in large-scale from the readily available starting materials.

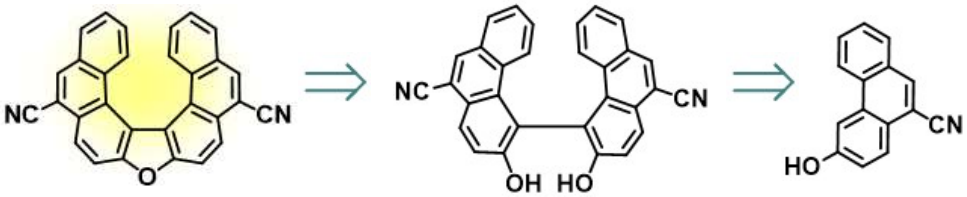

Target molecule

***Figure 3.3**: Retrosynthetic analysis of dicyano-9-oxa[7]helicene*

The Knoevenagel condensation of aldehydes with the substrate possessing active methylene group is one of the commonly used methods for the synthesis of olefins. 4-methoxy benzyl cyanide **51** was reacted with benzaldehyde **52** in presence of base in acetone at room temperature to afford the desired stilbene **53** in excellent yield. The stilbene derivative **53** was further subjected to oxidative photocyclization using stoichiometric amount of iodine and THF as HI scavenger in toluene.[21] The resulting solution was irradiated by a 250W HPMVL and the phenanthrene derivative **54** was isolated in excellent conversion (**Scheme 3.14**). The formation of **54** was confirmed by the disappearance of the olefinic proton in its ^{1}H NMR.

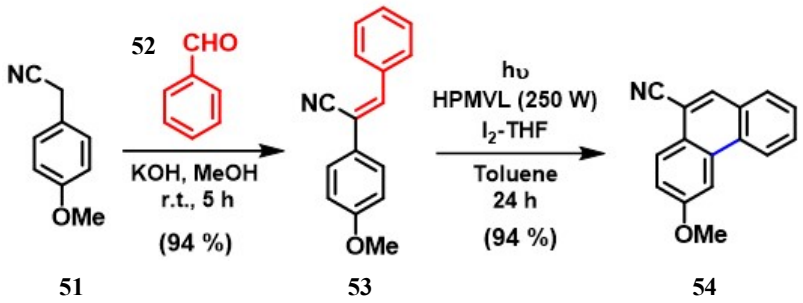

***Scheme 3.14**: Synthesis of 3-methoxyphenanthrene-10-carbonitrile*

The key step in the synthesis of our target molecule **50** involves oxidative homocoupling of 3-hydroxyphenanthrene derivative. For this purpose, we proceeded to cleave methoxy group to access the 3-hydroxyphenanthrene-10-carbonitrile **55**. Several known methods of cleavage of the methoxy group were investigated, but satisfactory results were not observed. The cleavage reaction did not proceed in presence of BBr_3 in dichloromethane,[22] gave poor yields with HBr-Acetic acid[23] or LiBr in DMF.[20] Subsequently the reaction proceeded well with $AlCl_3$-DMF and hydroxyl derivative **55** was isolated in moderate yield (**Scheme 3.15**, **Table 3.1**).[24]

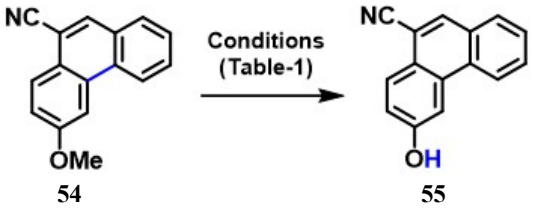

***Scheme 3.15**: Synthesis of 3-hydroxyphenanthrene-10-carbonitrile*

No.	Reagents and Solvent	Temperature	55 (% yield)	54 (% yield)
1	BBr_3 in DCM	0 °C to r.t.	0	100
2	LiBr in DMF, 4Å MS (100% w/w)	180 °C	23	77
3	HBr-Acetic acid	120 °C	46	38
4	**$AlCl_3$ in DMF**	**180 °C**	**68**	**32**

***Table 3.1**: Conditions for the cleavage of methoxy group of 54*

The formation of 3-hydroxyphenanthrene-10-carbonitrile **55** was confirmed by the disappearance of the signal for methoxy protons and marked by an appearance of broad singlet at 5.47 ppm in its ^{1}H NMR. The IR spectra showed a sharp band at ν 2228 cm^{-1} indicating that the cyano group is intact and not cleaved under these conditions of deprotection step.

Oxidative biaryl coupling between two aromatic phenols in presence of transition metal salts or some complexes is one of the most widely used approach to generate biaryls with a stereogenic axis. Some of the well-known transition metal systems used in the formation of C-C bonds are Fe(III),[15,25] Mn(III),[26] Cu(II)- amine,[27] CuCl(OH)-TMEDA/O_2,[28] V complexes[29] etc. The C-C homocoupling of **55** proceeded smoothly with the standard reagent of Cu-TMEDA[28,30] in methanol and a single regioisomer of diol **56** was obtained in good yield (**Scheme 3.16**).

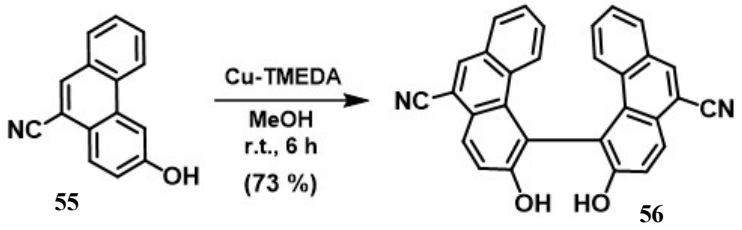

***Scheme 3.16**: Synthesis of bis-phenanthrol 56*

The mechanism of such C-C oxidative coupling reactions often shows the possibility of formation of a mixture of regioisomers as coupling can occur at C2 or C4 as both the positions are activated due to the presence of neighboring –OH group. Here, the coupling reaction proceeds regioselectively at C4 position of **55** as it generates the stabilized benzylic radical (**Scheme 3.17**). The reaction also involves the formation of keto dimer intermediate which rapidly undergoes keto-enol tautomerism to obtain the corresponding bis-phenanthrol derivative as the only product. The ^{1}H NMR of the product showed only half the number of expected signals indicating it to be symmetrical in nature. Also, the signal for the proton attached to C4 has disappeared. Thus we achieved the synthesis of precursor diol **56**, which will give us the target compound **50** by dehydration reaction.

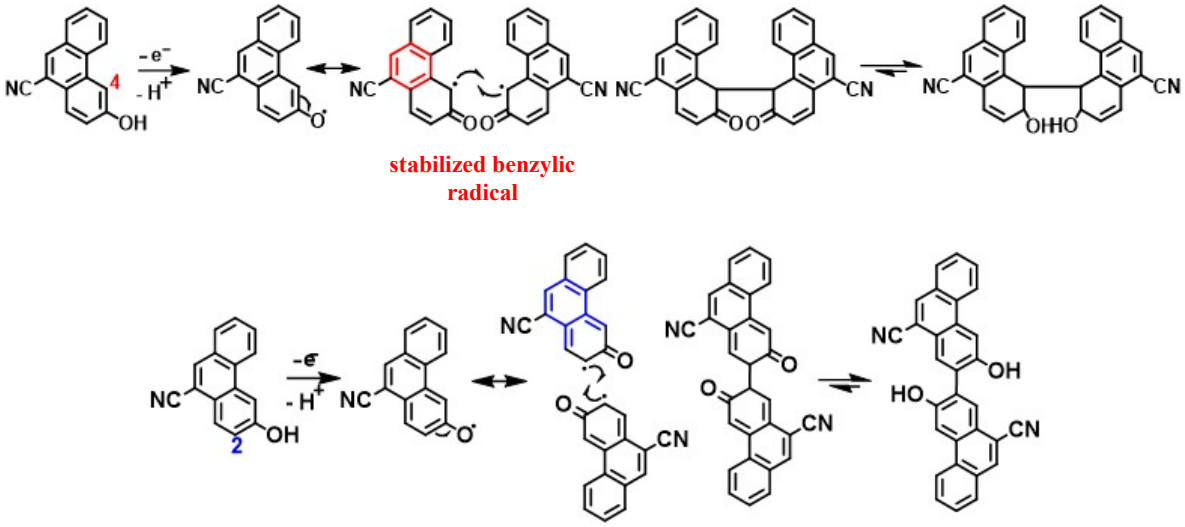

***Scheme 3.17**: Understanding regioselectivity of C-C homocoupling reaction*

Attempts to conduct acid catalyzed dehydration reaction of **56** with *p*-TSA, conc. H_2SO_4 and some solid acidic catalysts, resulted in either no reaction or formation of decomposed byproducts. Although we were unable to identify byproducts, the presence of the acidic sensitive cyano group may have caused these difficulties. Hence, we adopted a known method of effecting this type of cyclization by activating one of the hydroxyl groups. This activation is achieved by converting the hydroxyl group to mono nonafluorobutanesulfonate **57**, by treatment with perfluoro-1-butanesulfonyl fluoride and triethyl amine.[31] This activation of one of the hydroxyl groups was necessary to facilitate the nucleophilic attack in the formation of furan ring. This activated hydroxyl derivative **57** was subjected to palladium catalyzed cyclization with $Pd(OAc)_2$-Xantphos-Cs_2CO_3 system (**Scheme 3.18**). The helicene **50** was isolated by column chromatography over silica gel, and was characterized by usual spectral analysis. The ^{1}H NMR of **50** showed the signals specific for helicene. The protons attached to C2 and C16 appear in the most upfield region, at 6.40 ppm as they fall under the terminal benzene rings and hence shielded due to anisotropy.

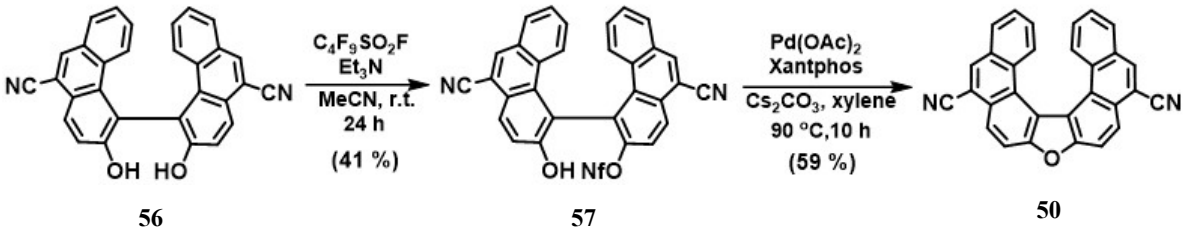

56 **57** **50**

***Scheme 3.18**: Cyclization of bis-phenanthrol 56*

3.3.2 Effect of change in the position of cyano groups

The ^{1}H NMR spectra of **50** indicated not only the formation of the desired angular-angular cyclization but the effect of change in the position of cyano group on the electronic nature of hydrogen at C-5 (& C-13) (**Figure 3.4**). The hydrogen at C-6 / C-12 in the case of **48** appeared at δ 9.03, while the protons attached to C-5 / C13 shifted to δ 8.86 (DMSO-d_6).

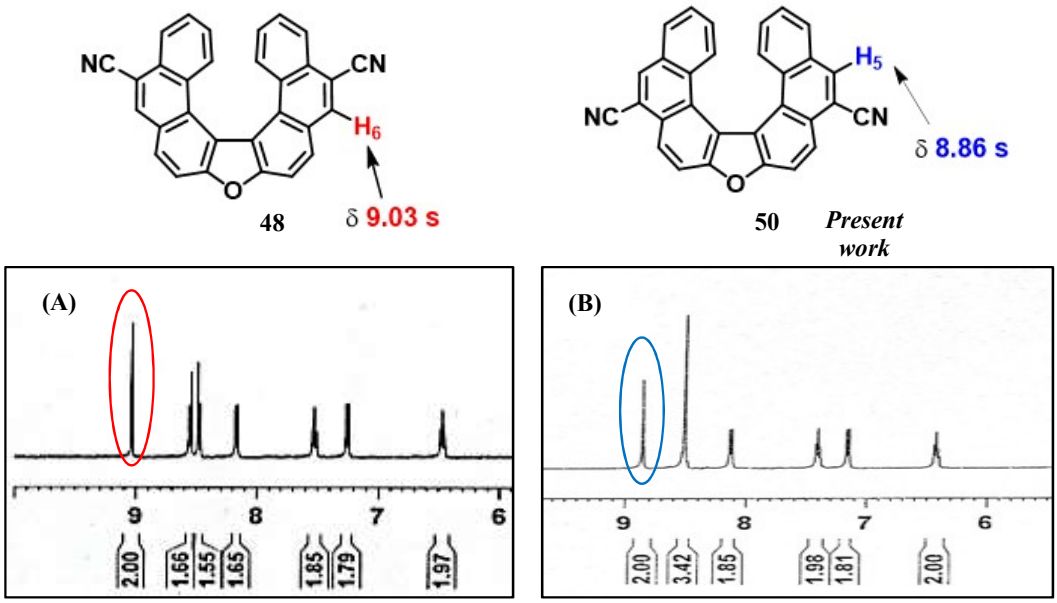

***Figure 3.4**: Comparision of the expanded aromatic region of ^1H NMR spectra in d_6-DMSO of (A) helicene 48 (B) helicene 50*

The appearance of signal at more down field region in **48** can be expected because of the pronounced deshielding effect of oxygen.

Another major difference was observed in their solubility. Compound **48** had poor solubility in most of the organic solvents, except DMSO.[20] However, the present isomer **50** was found to be readily soluble in many organic solvents, like dichloromethane, chloroform, 1,2-dichloroethane, toluene, chlorobenzene, and poorly soluble in acetone, ethylacetate, acetonitrile, THF, diethylether and alcohols. By looking at these differences in their solubility, we focused our efforts for its crystallization to study the spontaneous resolution. Various experiments of crystallization were performed for helicene **50**: chlorinated solvents, pure and in combination resulted in the thin hair-like crystals with no enrichment of isomers, amorphous solid was observed in case of chlorobenzene and good quality crystals were obtained only in case of toluene. However, to our disappointment no enrichment of isomers was seen in HPLC analysis.

3.3.3 X-ray Structure Analysis of compound 50

The crystal of compound **50** obtained from toluene was subjected to single crystal X-ray diffraction analysis. The ORTEP diagram of the crystal analysis is given in **Figure 3.5**. The compound **50** was crystallized in the $P2_1/n$ space group, its unit cell consists of eight molecules with equal number of *P* and *M* isomers. The width of the molecule, from nitrogen to nitrogen

of dicyano is about 13.11 Å (**Table 3.2)**. The interplanar angle was found to be 27.85° which is smaller compared to some of the 2,16-disubstituted aza[7]helicenes.[32] The torsional angles between the inner carbon atoms of **50** were found to be 17.85°, 19.05° and 11.46° indicating different degrees of distortion in the *ortho* fused aromatic rings. The sum of the three dihedral angles φ1, φ2 and φ3 was observed to be 48.36°, which provides considerable stability to the isomers. Indeed, the two isomers were well separated on chiral phase HPLC analysis (Chiralcel OD-H; IPA in hexane (20%); 1.0 mL/min; two peaks at 15.3 and 17.0 min.). The direct consequence of this distortion created by the helical twist is seen in the deviation of the bond lengths of rings. Compared to the standard bond length of benzene (1.393 Å), the range of the inner carbon-carbon bond length is observed to be larger (1.408-1.471 Å) while the same in outer periphery was seen to be smaller (1.367-1.372 Å). The intramolecular helical pitch, the distance between the periphery carbon pair, was seen to be 4.166 Å in **50**.

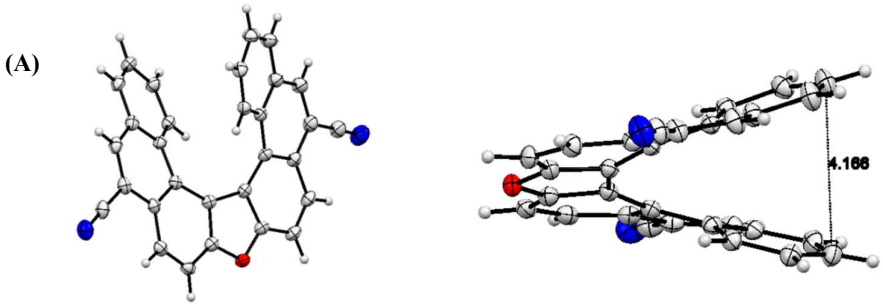

***Figure 3.5**: (A) ORTEP Diagram of 50 (CCDC-2113912) (B) intramolecular helical pitch*

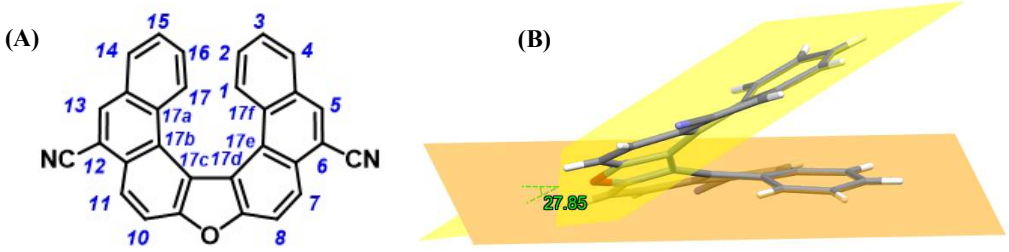

***Figure 3.6**: (A) Numbering Scheme in 50 (B) figure showing interplanar angle*

Inner carbon-carbon bond length (Å)	
C17c-C17d	1.471
C17d-C17e	1.425
C17e-C17f	1.455
C17f-C1	1.408
Outer carbon-carbon bond length (Å)	
C3-C4	1.370
C5-C6	1.367
C7-C8	1.372
Torsion angle (°)	
φ1 = C17-C17a-C17b-C17c	17.85
φ2 = C17a-C17b-C17c-C17d	19.05
φ3 = C17b-C17c-C17d-C17e	11.46
Distortion of the molecular structure (°)	
φ1 + φ2 + φ3	48.36
Dihedral angle θ (°)	27.85
Intramolecular pitch of the helicene	4.166
Width of the molecule, from N to N of dicyano (Å)	13.11

***Table 3.2**: Selected X-ray crystallographic data of compound 50*

The single crystal of oxahelicene **50** depicts a typical (π–π) interaction resulting in stacking of molecules on top of each other. The molecules are held together at a distance of (3.403 Å) (**Figure 3.7**).

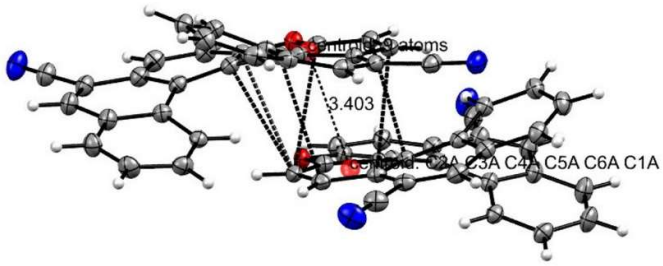

***Figure 3.7**: Intermolecular π–π interaction in the crystal packing of 50*

In addition, the crystal structure exhibits strong intermolecular lateral interactions between the furan ring oxygen 'O' and hydrogen of adjacent ring (CH-O) (2.434 Å). Interestingly, similar lateral interaction is observed between the furan ring oxygen 'O' of the second molecule with the hydrogen of adjacent ring of first molecule (CH-O) (2.434 Å), thereby holding the two molecules together. Furthermore, the distance between interactions is also identical. In addition,

similar interaction is observed between the cyano nitrogen 'N' and two hydrogen atoms from adjacent carbon and adjacent ring (CN-HC) (2.682 & 2.693 Å) respectively. Similar interaction between the cyano nitrogen 'N' of second molecule and two hydrogen atoms from adjacent carbon and adjacent ring of the first molecule (CN-HC) (2.682 & 2.693 Å) respectively is also witnessed (**Figure 3.8 (A)**).

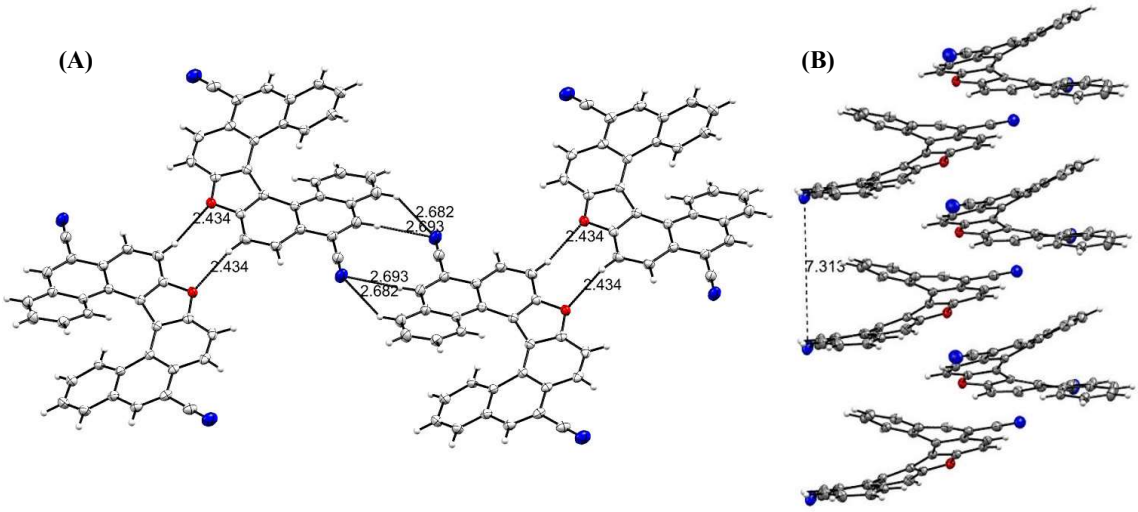

***Figure 3.8**: (A) Intermolecular lateral interactions in the crystal packing of 50 (B) Stacking of molecules in a single column*

The single crystal further exhibits stacking of molecules attributing to lateral interactions (CH-O & CN-HC) and (π–π) interactions resulting in columnar structures. The (**Figure 3.8 (B)**) indicates that the nitrogen 'N' from cyano groups of overlying molecules, in a single column, are separated by a distance of 7.313 Å. Each column, having width of 15.792 Å, consists of two rows of molecules held by lateral interaction (CH-O & CN-HC).

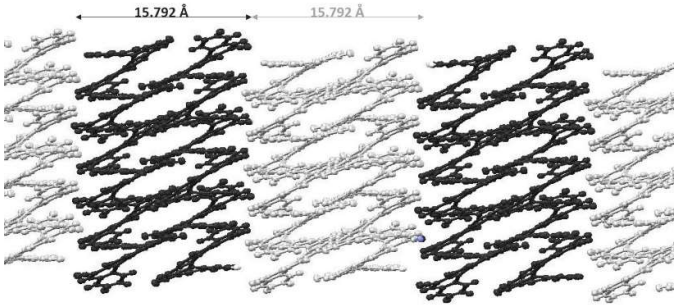

***Figure 3.9**: Columnar packing observed in molecular assembly of 50*

3.3.4 Photophysical properties of compound 50

The photophysical properties of **50** were then investigated by UV-Vis absorbance and

florescence spectral study and compared to that of compound **48** (**Figure 3.10**, **Table 3.3**).

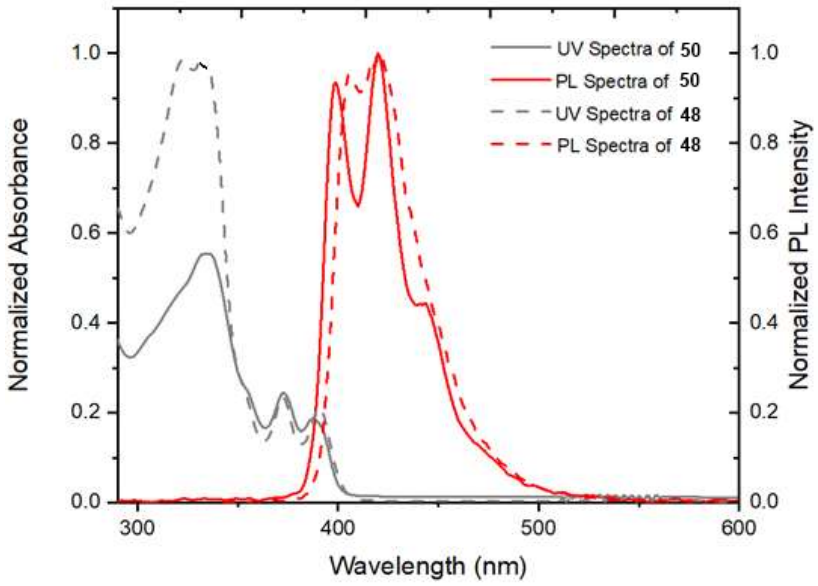

***Figure 3.10**: UV-Vis (10^{-5} M) and Fluorescence (1.5×10^{-6} M) spectra of 48 (dash line) and 50 (solid line), in DMSO*

Compound **50** showed absorption maxima at 335 nm along with two other bands at 373 and 388 nm in DMSO at ambient temperature. For a similar helicene **48**, a blue shift of 12 nm was observed in its absorption maxima, λ_{max} for compound **48** was found to be 323 nm. This led to decrease in the value of Stokes shift of compound **50** (85 nm), compared to compound **48** (98 nm) as the emission maxima of both helicenes **50** and **48** were observed at 420 and 421 nm respectively.

Compound	**λ_{abs} (nm)**	**λ_{ems} (nm)**	**Stokes shift (nm)**
48	323, 334, 372, 391	421	98
50	335, 373, 388	399, 420	85

***Table 3.3**: Comparison of photophysical properties of 3 and 4*

The absorption and emission values were in the expected range for such type of helical systems.[33] The photophysical properties of compound **50** were further studied in solvents of different polarity (**Figure 3.11**, **Table 3.4**). Absorption behavior of compound **50** in toluene, chlorobenzene, chloroform, dichloroethane and dimethylacetamide resembled those of in dimethylsulfoxide with absorption maxima ranging from 332-335 nm. A solvent change from

toluene to dimethylsulfoxide caused small shifts of 1-3 nm in the absorption bands. Also similar trend was observed in case of photoluminescence spectra as the peaks for emission maxima ranges from 417-420 nm. Thus, photophysical behavior of compound **50** was independent of solvent polarity.

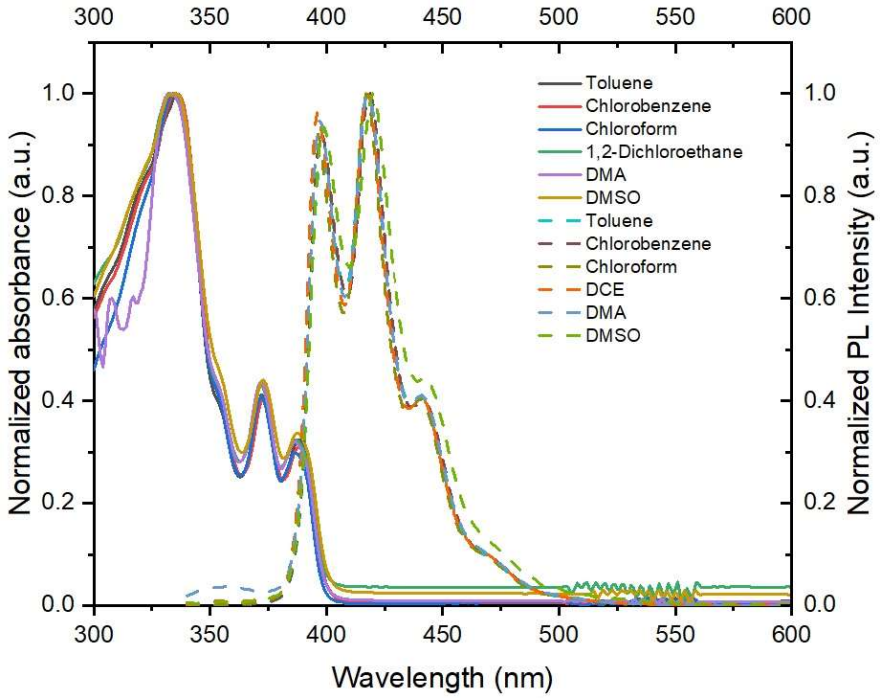

***Figure 3.11**: UV-Vis (10^{-5} M) and Fluorescence (1.5 X 10^{-6} M) spectras of compound 50 in different solvents*

Solvent	λ_{abs} (nm)	λ_{ems} (nm)	Stokes shift (nm)
Toluene	335, 372, 388	398, 418, 441	83
Chlorobenzene	335, 372, 388	398, 419, 442	84
Chloroform	333, 372, 387	396, 417, 441	84
1,2-Dichloroethane (DCE)	334, 372, 387	396, 418, 440	84
***N,N*-Dimethylacetamide (DMA)**	307, 317, 332, 372, 386	397, 418, 441	86
Dimethylsulphoxide (DMSO)	335, 373, 388	399, 420, 443	85

***Table 3.4**: UV-Vis (10^{-5} M) and Fluorescence (1.5 X 10^{-6} M) data of compound 50 recorded in solvents of different polarity at room temperature*

3.3.5 *Computational Analysis of compound 50*

Optimization of the structure of compound **50** was done at B3LYP/6-31G level of theory using Gaussian 09 Software (**Figure 3.12**). The calculations of bond lengths, bond angles, intramolecular helical pitch, were in close agreement to the results obtained from the X-ray crystallographic data. However, the dihedral angle for **50**, predicted from the theoretical data was 38.82° (in vacuum) and 38.75° (in toluene), while from the X-ray crystallographic data it was found to be 27.85°.

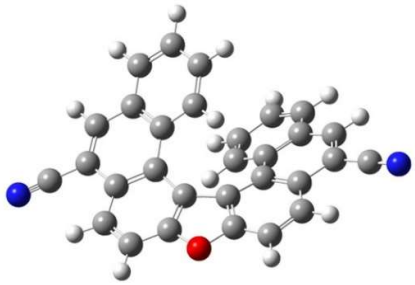

Figure 3.12: Optimized molecular structure of 50 calculated at the B3LYP/6-31G level of theory

For helicenes, the frontier molecular orbital (FMOs) distributions and energy gap (HOMO-LUMO gap) are closely associated to electronic and optical properties. The energy gap between the highest occupied molecular orbital (HOMO) and the lowest unoccupied molecular orbital (LUMO) of helicene **50** was calculated from its UV-vis absorption edge with the help of the Tauc plot method[34] and was found to be around 3.13 eV, which is a characteristic value of a wide-band gap semiconductor. The theoretical HOMO-LUMO gap which was obtained by the density functional theory (DFT) calculations using the B3LYP/6-31G level of theory for compound **50** was 3.88 eV. The HOMO and LUMO energy levels were calculated to be -6.13 and -2.25 eV, respectively in vacuum for compound **50** (**Figure 3.13**).

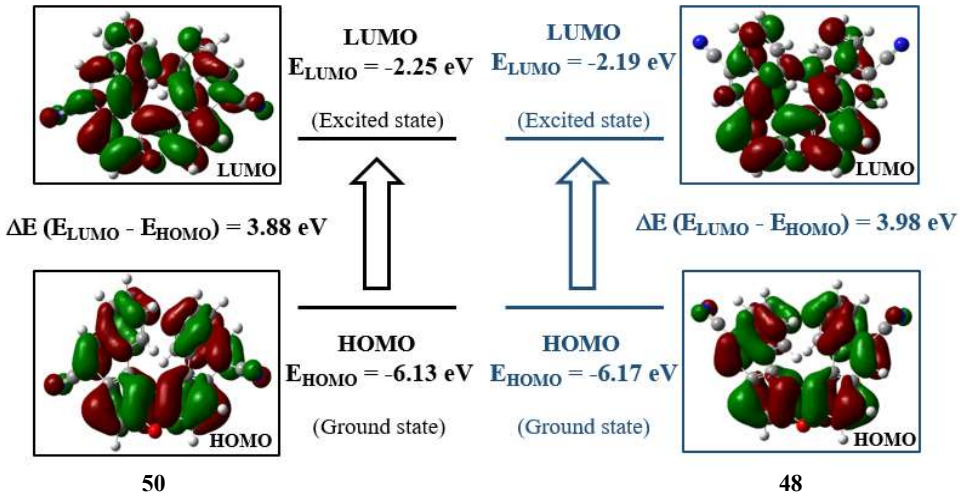

Figure 3.13: HOMO and LUMO orbitals of compound 50 (left, in black) and compound 48 (right, in blue) calculated at B3LYP/6-31G level of theory

Similarly, the HOMO-LUMO band gap energy for compound **48** calculated using the B3LYP/6-31G level of theory was found to be 3.98 eV, the HOMO and LUMO energy levels being -6.17 and -2.19 eV respectively (**Figure 3.13**). The band gap energy for compound **48** calculated from its UV-vis absorption edge with the help of Tauc plot method was found to be 3.03 eV. The band gap energy calculated for compound **48** from experimental and theoretical data was quite comparable to the one, obtained for compound **50**.

3.3.6 *Thermal properties of compound 50*

The thermogravimetric analysis showed that the helicene **50** possessed a high thermal-decomposition temperature (T_d) of 328 °C (**Figure 3.14 (A)**). It is to be noted that a high T_d value is an asset to OLED applications. DSC scans were performed, where the sample was heated at the rate of 10 °C /min from 40 to 280 °C under N_2 atmosphere. During this heating process, an endothermic peak was not observed which indicates that the melting point of compound **50** is greater than 280 °C (**Figure 3.14 (B)**). These thermal analysis data indicated high thermal stability of compound **50**.

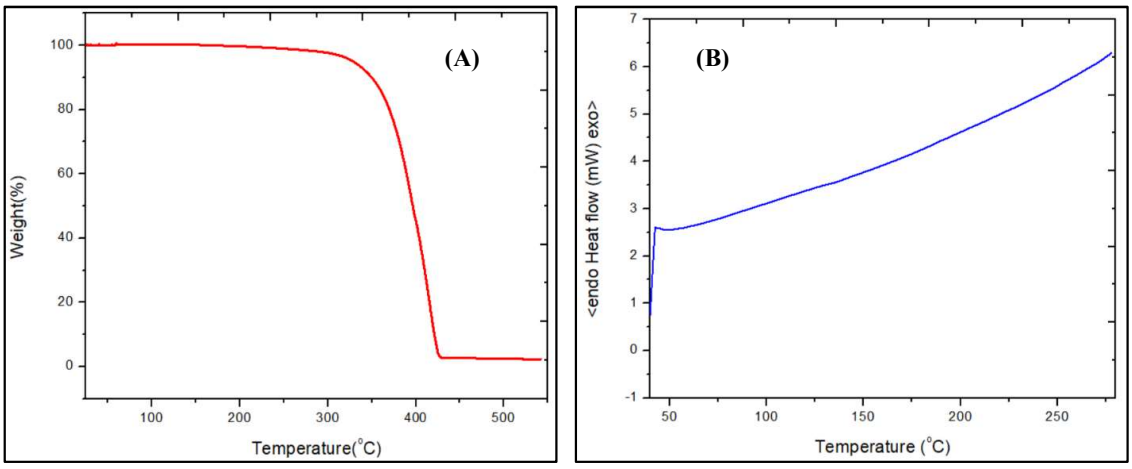

***Figure 3.14**: (A) TGA curve of compound 50 (B) DSC thermogram of compound 50*

3.4 Conclusion

In this chapter we have presented the synthesis and study of 6,12-dicyano-9-oxa[7]helicene. The helicene was synthesized by Pd catalyzed intramolecular cyclization of the

activated bis-phenanthrol derivative. With the aim to study spontaneous resolution, various experiments of crystallization were performed and the crystal obtained in toluene was studied in detail by single crystal X-ray diffraction. However, our efforts to effect separation of isomers by spontaneous resolution did not meet with success. In comparision with its analogue 5,13-dicyano-9-oxa[7]helicene, we have observed changes in the overall solubility of the compound, its photophysical properties and shifting of signals in the ^{1}H NMR. The synthesized helicene also showed good thermal stability. Its geometry optimization was carried out using B3LYP/6-31G level of theory and HOMO-LUMO energy gap was also calculated.

3.5 Experimental Data

Reagents were purchased from Sigma-Aldrich Chemicals Limited, Sisco, Avara Chemicals Limited, etc., and were used without further purification. Thin layer chromatography was performed on Merck 60 F254 Aluminum coated plates. The spots were visualized under UV light or with iodine vapor. All the compounds were purified by column chromatography using SRL silica gel (60–120 mesh). All reactions were carried out under an inert atmosphere (nitrogen) unless other conditions are specified. NMR Spectra were recorded on a 400 MHz Bruker Advance 400 spectrometer (400 MHz for ^{1}H NMR, 100 MHz for ^{13}C NMR and 376 MHz for ^{19}F NMR) with $CDCl_3$ as the solvent and TMS as the internal standard. Signal multiplicity is denoted as singlet (s), broad singlet (bs), doublet (d), doublet of doublet (dd), triplet (t), doublet of triplet (dt), quartet (q), and multiplet (m). Mass spectra were recorded on a Thermo-Fischer DSQ ll GCMS instrument. IR Spectra were recorded on a Perkin-Elmer FTIR RXI spectrometer as KBr pellets. UV-vis spectra were recorded on Perkin-Elmer Lambda-35. Fluorescence spectra were recorded on a JASCO FP-6300 spectrofluorometer. Melting points were recorded in Thiele's tube using paraffin oil and are uncorrected.

Synthetic procedures and analytical data

2-(4-Methoxyphenyl)-3-phenylacrylonitrile (53)

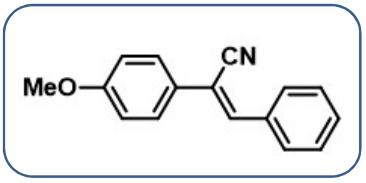

Molecular formula: $C_{16}H_{13}NO$
Molecular weight: 235.28
Physical state: white crystalline solid
M.p = 94 °C

A mixture of *p*-methoxybenzyl cyanide **51** (3.0 g, 2.8 mL, 20.7 mmol), finely grounded KOH (2.1 g, 37.6 mmol) and benzaldehyde (2.0 g, 1.9 mL, 18.8 mmol) in methanol (30 mL) was stirred at room temperature for 6 hours. The resultant reaction mixture was concentrated under reduced pressure, poured into water and extracted using ethyl acetate (3 X 50 mL). The combined organic layer was dried over anhydrous sodium sulphate. The concentrated mixture was purified on silica gel column using petroleum ether/ ethyl acetate (95:5) to afford **53** as white solid. The analytical data were in complete agreement with the previously published data.[35] **Yield:** 4.1 g (94%)

^{1}H NMR (400 MHz, $CDCl_3$): δ 7.89 (dd, *J* = 7.2 and 1.6 Hz, 2H), 7.65-7.62 (m, 2H), 7.50-7.41 (m, 4H), 7.00-6.96 (m, 2H), 3.87 (s, 3H).

IR (KBr): 3004, 2839, 2214, 1606, 1571, 1510, 1465, 1441, 1351, 1255, 1180, 1031, 834,

770, 746, 694, 531, 432 cm^{-1}.

MS (DIP-EI): *m/z* 235 (M^+,100%), 219 (23%), 204 (32 %), 190 (26%), 165 (57%), 85 (19%), 83 (36%).

3-Methoxyphenanthrene-10-carbonitrile (54)

Molecular formula: $C_{16}H_{11}NO$
Molecular weight: 233.27
Physical state: pale yellow solid
M.p = 158 °C

A solution of **53** (1.0 g, 4.25 mmol) and iodine (1.18 g, 4.68 mmol) in toluene (1250 mL) and tetrahydrofuran (17.0 mL, 210.3 mmol, 50 equivalent) was irradiated in a standard immersion well photoreactor with 250W high pressure mercury vapour lamp for 48 hours. The reaction mixture was then washed with aqueous sodium thiosulphate and dried over anhydrous sodium sulphate. The concentrated mixture was purified on silica gel column using petroleum ether/ ethyl acetate (95:5) to afford **54** as pale yellow solid. The analytical data were in complete agreement with the previously published data.[35] **Yield:** 0.93 g (94%)

^{1}H NMR (400 MHz, $CDCl_3$): δ 8.62 (d, *J* = 8.4Hz, 1H), 8.22 (d, *J* = 8.8Hz, 1H), 8.12 (s, 1H), 8.06 (d, *J* = 2.8Hz, 1H), 7.94-7.92 (m, 1H), 7.81-7.77 (m, 1H), 7.71-7.67 (m, 1H), 7.39 (dd, *J* = 8.8 and 2.4Hz, 1H), 4.06 (s, 3H).

IR(KBr): 3065, 2974, 2948, 2843, 2218, 1617, 1524, 1505, 1441, 1388, 1229, 1146, 1020, 893, 851, 816, 743, 622, 531, 456, 427 cm^{-1}.

MS (DIP-EI): *m/z* 233 (M^+, 5%), 190 (8%) 149 (21%), 129 (68%), 111 (28%), 83 (55%), 69 (83%), 57 (100%).

3-Hydroxyphenanthrene-10-carbonitrile (55)

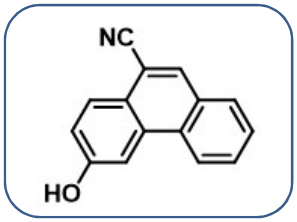

Molecular formula: $C_{16}H_{11}NO$
Molecular weight: 233.27
Physical state: pale yellow solid

To a round bottom flask was added **54** (0.663 g, 2.72 mmol) and anhydrous aluminium chloride $AlCl_3$ (1.81 g, 13.58 mmol) in dimethyl formamide (50 mL, followed by heating in an oil bath

to 180 °C for 24 hours). The reaction mixture was then allowed to cool to room temperature. Water was added to the reaction mixture and it was allowed to stand till the solution becomes clear. It was extracted using ethyl acetate (3 X 50 mL). The combined organic layer was dried over anhydrous sodium sulphate and concentrated under reduced pressure. The concentrated mixture was purified on silica gel column using petroleum ether/ ethyl acetate (80:20) to afford **55** as pale yellow solid. **Yield:** 0.42 g (68%); Melting Point: above 220 °C.

^{1}H NMR (400 MHz, $CDCl_3$): δ 8.57 (d, *J* = 8.0Hz, 1H), 8.22 (d, *J* = 8.8Hz, 1H), 8.14 (s, 1H), 8.09 (d, *J* = 2.0Hz, 1H), 7.94 (d, *J* = 8.0Hz, 1H), 7.81-7.77 (m, 1H), 7.71-7.67 (m, 1H), 7.32 (dd, *J* = 8.8 and 2.4Hz, 1H), 5.46 (s, 1H).

^{13}C NMR (100 MHz, $CDCl_3$): δ 107.97, 116.53, 118.12, 123.48, 126.72, 127.84, 128.00, 128.88, 129.48, 129.68, 130.70, 131.93, 139.81, 154.84, 155.64.

IR(KBr): 3361, 2228, 1616, 1537, 1503, 1442, 1391, 1349, 1230, 1204, 884, 841, 819, 742, 623, 602, 531, 424 cm^{-1}.

MS (DIP-EI): *m/z* 219 (M^+, 100%), 190 (40%), 109 (20%).

HRMS (TOF MS ES+): *m/z* calcd for $C_{15}H_{10}NO[M+H]^+$ 220.0684, found 220.0758.

3,3'-Dihydroxy-[4,4'-biphenanthrene]-10,10'-dicarbonitrile (56)

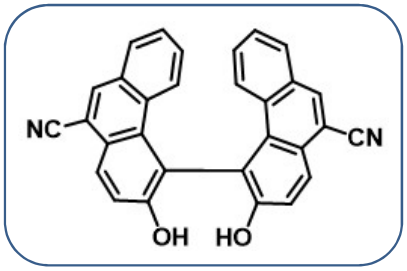

Molecular formula: $C_{30}H_{16}N_2O_2$
Molecular weight: 436.47
Physical state: white solid

In a 50 mL round bottom flask, a mixture of 3-hydroxyphenanthrene-9-carbonitrile **55** (0.2g,0.9 mmol), $CuCl(OH)[(Me_2N)_2CH_2CH_2(NMe_2)_2]$ (0.21 g, 0.9 mmol) in methanol (25 mL) was placed and was sonicated for 10 mins. The reaction mixture was stirred at room temperature. The reaction mixture was concentrated to remove methanol and 1M aqueous HCl was added. The resulting mixture was extracted with ethyl acetate (3 X 50 mL). The organic layer was dried over anhydrous sodium sulphate, filtered and concentrated under reduced pressure. Purification of the crude residue by silica gel column chromatography with petroleum ether/ ethyl acetate (70:30) as an eluent gave **56** as a colourless solid. **Yield:** 0.145g (73%); Melting Point: above 220 °C.

^{1}H NMR (400 MHz, DMSO-*d*^{6}): δ 9.79 (s, 2H), 8.49 (s, 2H), 8.25 (d, *J* = 8.8Hz, 2H), 8.04-8.0 (m, 4H), 7.53 (d, *J* = 8.8Hz, 2H), 7.47 (t, *J* = 7.2Hz, 2H), 7.12-7.08 (m, 2H).

^{13}C NMR (100 MHz, DMSO-*d*^{6}): δ 109.34, 118.76, 119.35, 122.94, 123.67, 125.28, 127.17, 127.69, 129.23, 130.26, 131.01, 131.35, 132.52, 133.89, 155.35.

IR(KBr): 3359, 2923, 2233, 1595, 1496, 1443, 1395, 1223, 1157, 894, 826, 751, 611 cm^{-1}.

MS (DIP-EI): *m/z* 437 (M^+, 22%), 435 (89%), 392 (54%), 361 (100%), 343 (21%), 272 (46%), 188 (38%), 136 (44%).

HRMS (TOF MS ES+) *m/z* calcd for $C_{30}H_{17}N_2O_2[M+H]^+$ 437.1212, found 437.1276.

10,10'-dicyano-3'-hydroxy-[4,4'-biphenanthren]-3-yl-1,1,2,2,3,3,4,4,4-nonafluorobutane-1-sulphonate (57)

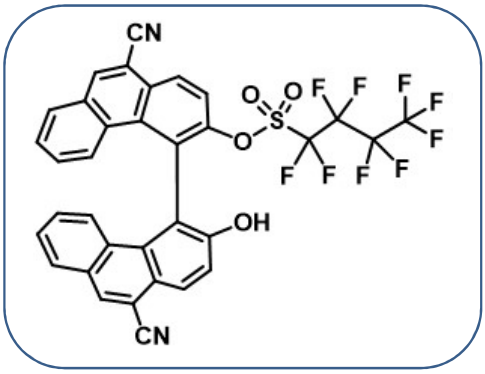

Molecular formula: $C_{34}H_{15}N_2O_4F_9S$
Molecular weight: 718.54
Physical state: white solid

Compound **56** (0.167 g, 0.38 mmol) was taken in a round bottom flask and dissolved in acetonitrile (10 mL). The solution was cooled to 0 °C and to this solution was slowly added triethylamine (0.061 mL, 0.46 mmol) and perfluoro-1-butanesulfonyl fluoride (0.082 mL, 0.46 mmol) at 0 °C. The reaction mixture was stirred at room temperature for 12 hours. The reaction mixture was concentrated to remove acetonitrile. The resulting mixture was extracted with ethyl acetate (3 X 50 mL). The organic layer is dried over anhydrous sodium sulphate, filtered and concentrated under reduced pressure. Purification of crude residue by silica gel column chromatography with petroleum ether/ ethyl acetate (85:15) as an eluent gave **57** white solid. **Yield:** 0.11g (41%); Melting Point: 120 °C.

^{1}H NMR (400 MHz, $CDCl_3$): δ 8.68 (d, *J* = 9.2Hz, 1H), 8.51 (d, *J* = 8.8Hz, 1H), 8.48 (s, 1H), 8.26-8.28 (m, 2H), 8.00 (dd, *J* = 7.8 and 1.4Hz, 1H), 7.93 (dd, *J* = 8.0 and 1.2Hz, 1H), 7.83 (d, 8.8Hz, 1H), 7.68 (d, *J* = 8.8Hz, 1H), 7.64-7.60 (m, 1H), 7.53-7.49 (m, 1H), 7.45 (d, *J* = 8.8Hz, 1H), 7.26-7.23 (m, 1H), 7.13-7.10 (m, 1H), 5.69 (bs, 1H).

^{19}F NMR (376 MHz, $CDCl_3$): δ -126.06 (m, 2F), -121.33 (m, 2F), -110.19 (m, 2F), -80.71 (t,

3F).

IR(KBr): 3381, 2923, 2226, 1651, 1615, 1574, 1494, 1446, 1423, 1352, 1295, 1239 1206, 1143, 1065, 915, 751, 585 cm^{-1}.

HRMS (ESI): *m/z* calcd for $C_{34}H_{15}N_2O_4F_9SNa[M+Na]^+$ 741.0609, found 741.0501.

Diphenanthro[3,4-b:4',3'-d]furan-6,12-dicarbonitrile (50)

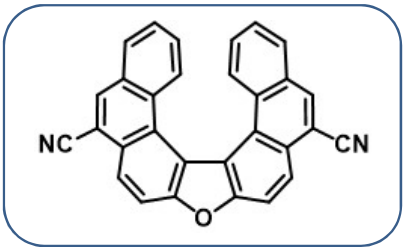

Molecular formula: $C_{30}H_{14}N_2O$
Molecular weight: 418.45
Physical state: pale yellow solid

A mixture of **57** (0.075 g, 0.10 mmol), $Pd(OAc)_2$ (0.001 g, 0.005 mmol), xantphos (0.012 g, 0.021 mmol), anhydrous Cs_2CO_3 (0.068 g, 0.20 mmol) in xylene (10 mL) was placed in a 50 mL round bottom flask and degassed by sonicating for 10 mins. The reaction mixture was stirred at 80 °C for 12 hours under nitrogen atmosphere. The reaction mixture was cooled down to ambient temperature and was then diluted with toluene (10 mL). The resulting mixture was washed with water, extracted with toluene, dried over anhydrous Na_2SO_4, filtered and concentrated under reduced pressure. The resulting crude residue was purified by silica gel column chromatography with petroleum ether/ethyl acetate (90:10) as an eluent to give **50** as a pale yellow solid. **Yield:** 0.026g (59%); Melting Point: above 220 °C.

^{1}H NMR (400 MHz, $CDCl_3$): δ 8.63 (d, *J* = 8.8Hz, 2H), 8.43 (s, 2H), 8.25 (d, *J* = 8.4Hz, 2H), 7.94 (d, *J* = 7.6Hz, 2H), 7.35 (t, *J* = 7.6Hz, 2H), 7.26 (d, *J* = 8.0Hz, 2H), 6.41 (t, *J* = 7.6Hz, 2H).
^{1}H NMR (400 MHz, DMSO-*d*^{6}): δ 8.86 (s, 1H), 8.513 (m, 4H), 8.13 (d, *J* = 8.0 Hz, 2H), 7.41 (t, *J* = 7.4 Hz, 2H), 7.16 (d, *J* = 8.4 Hz), 6.43 (t, *J* = 7.6 Hz).
^{13}C NMR (100 MHz, $CDCl_3$): δ 109.21, 113.36, 118.30, 118.61, 125.98, 126.01, 126.13, 126.80, 127.55, 127.89, 127.99, 129.35, 131.03, 134.36, 156.66.
IR(KBr): 3066, 2925, 2853, 2220, 1714, 1462, 1382, 1223, 814, 759 cm^{-1}.
MS (DIP-EI): *m/z* 418(M^+, 43%), 417(11%), 111(30%), 97(52%), 95(52%), 83(55%), 69(65%), 57(100%), 55(72%).
HRMS (ESI) m/z calcd for $C_{30}H_{14}N_2ONa$ $[M+Na]^+$ 441.4550, found 441.0995.

3.6 Spectral Data

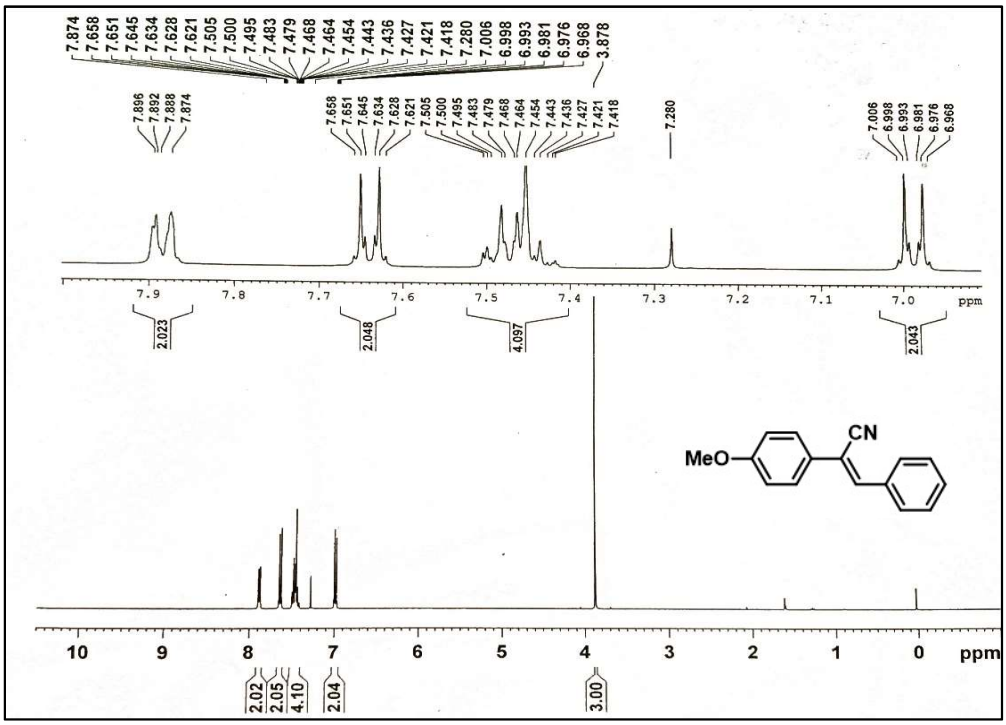

^{1}H NMR Spectrum of 53 ($CDCl_3$, 400 MHz)

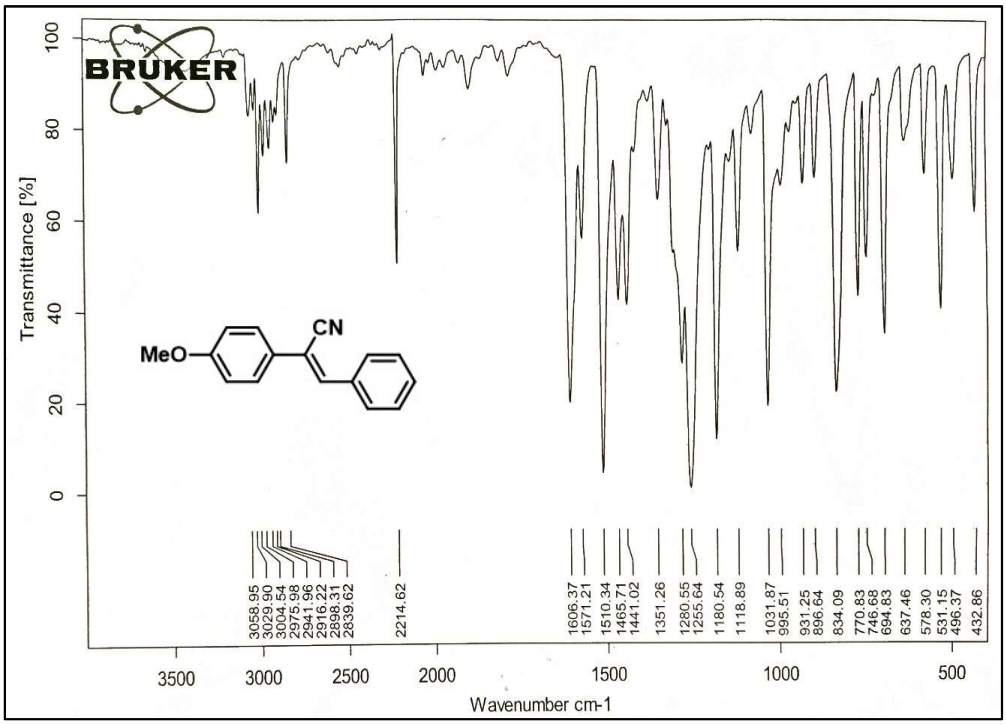

IR Spectrum of 53

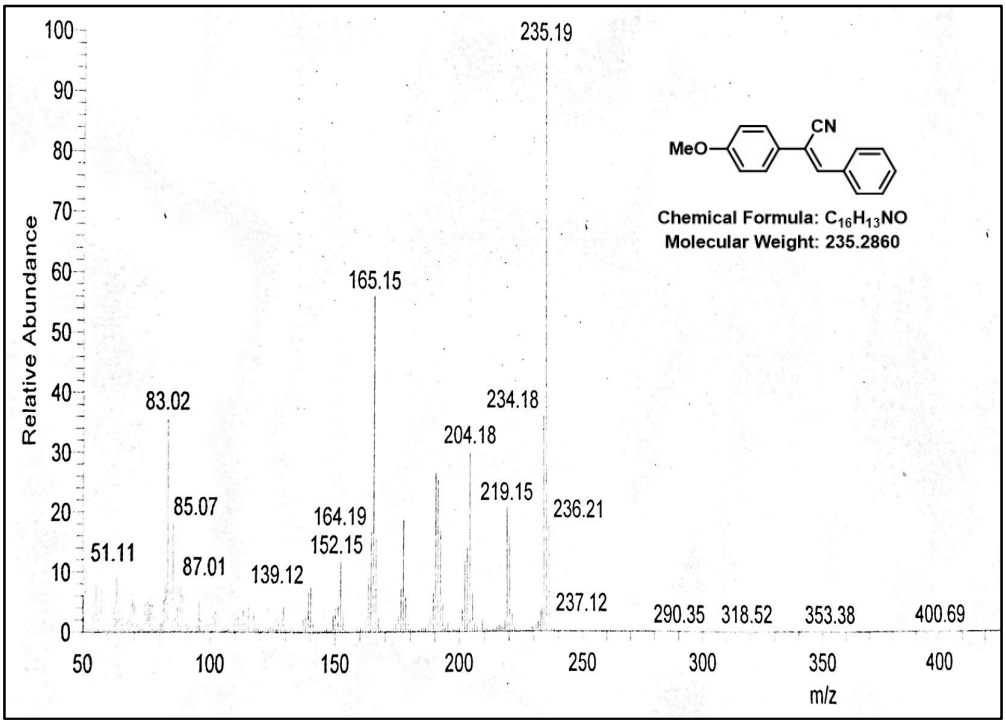

Mass Spectrum of 53

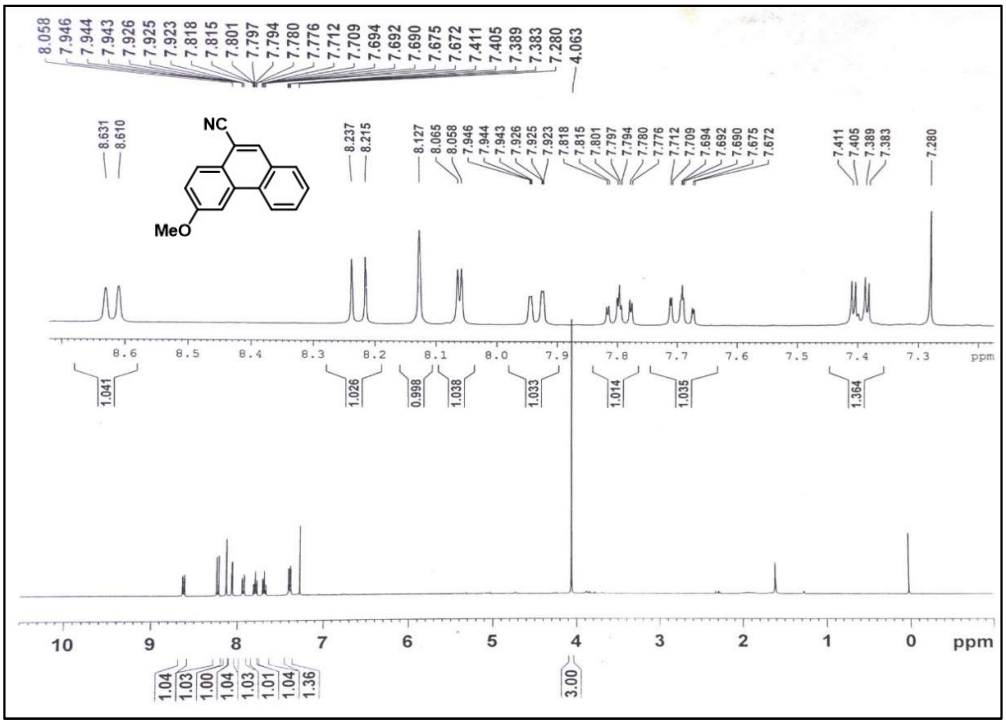

^{1}H NMR Spectrum of 54 ($CDCl_3$, 400 MHz)

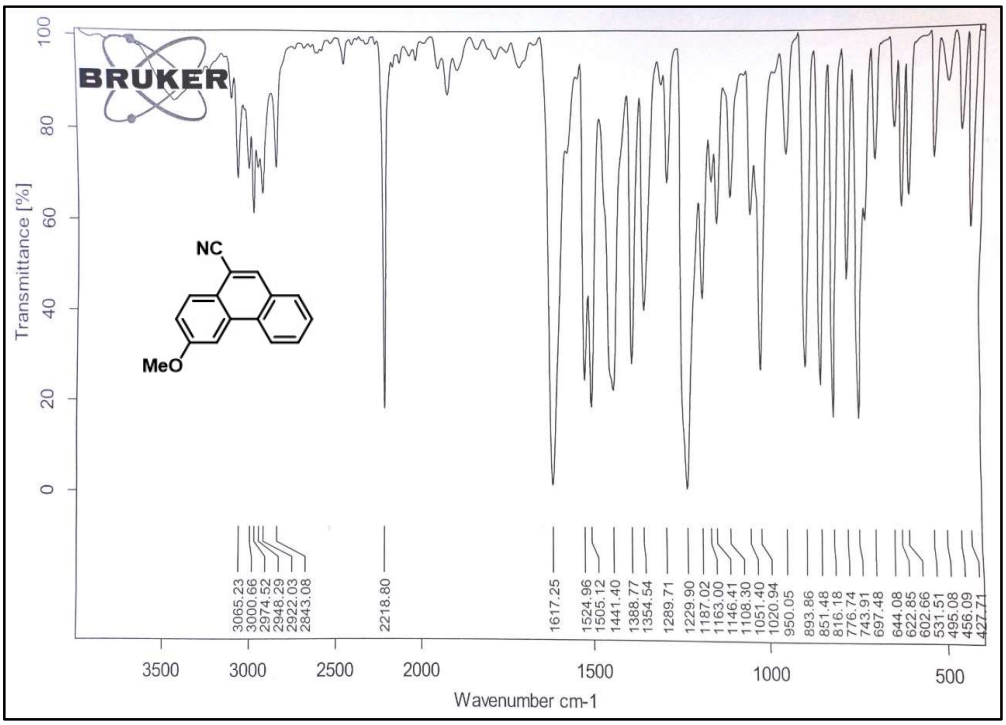

IR Spectrum of 54

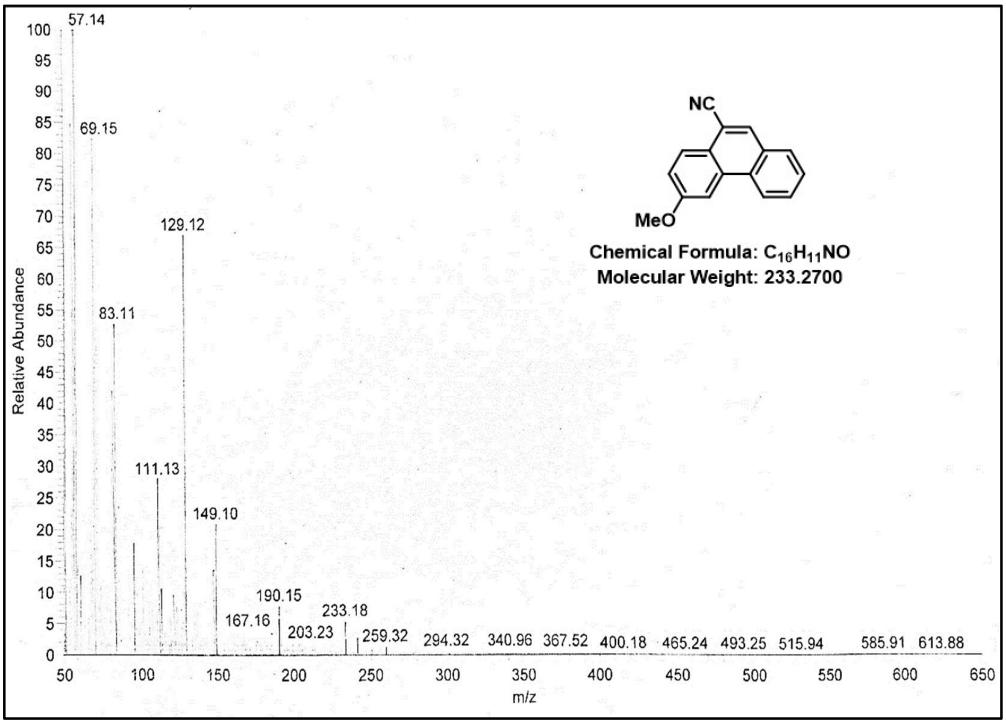

Mass Spectrum of 54

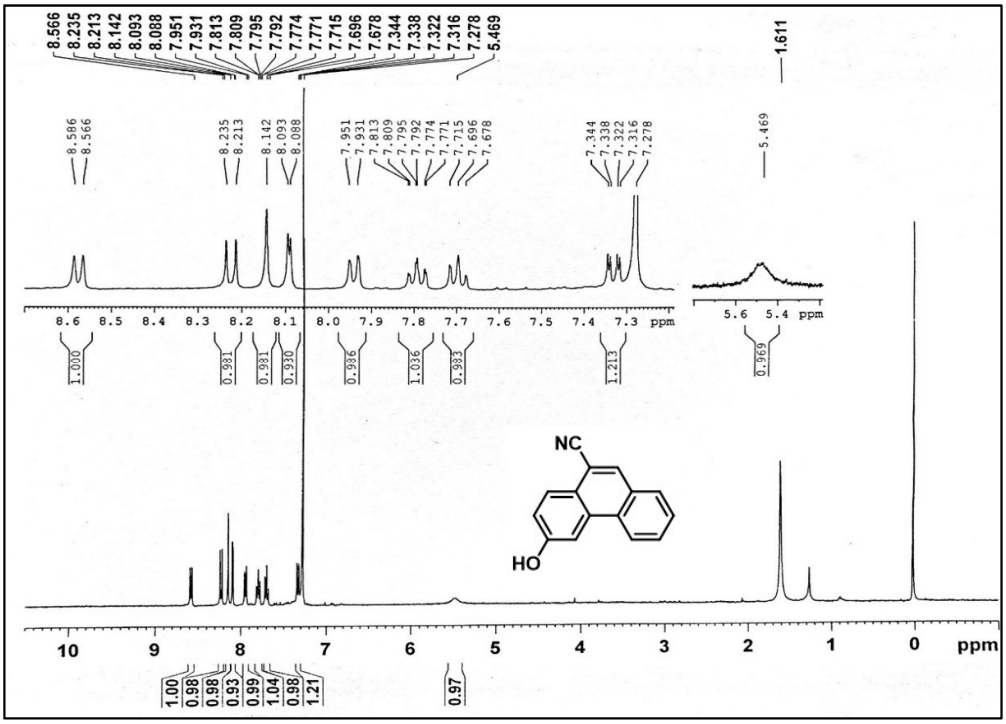

^{1}H NMR Spectrum of 55 ($CDCl_3$, 400 MHz)

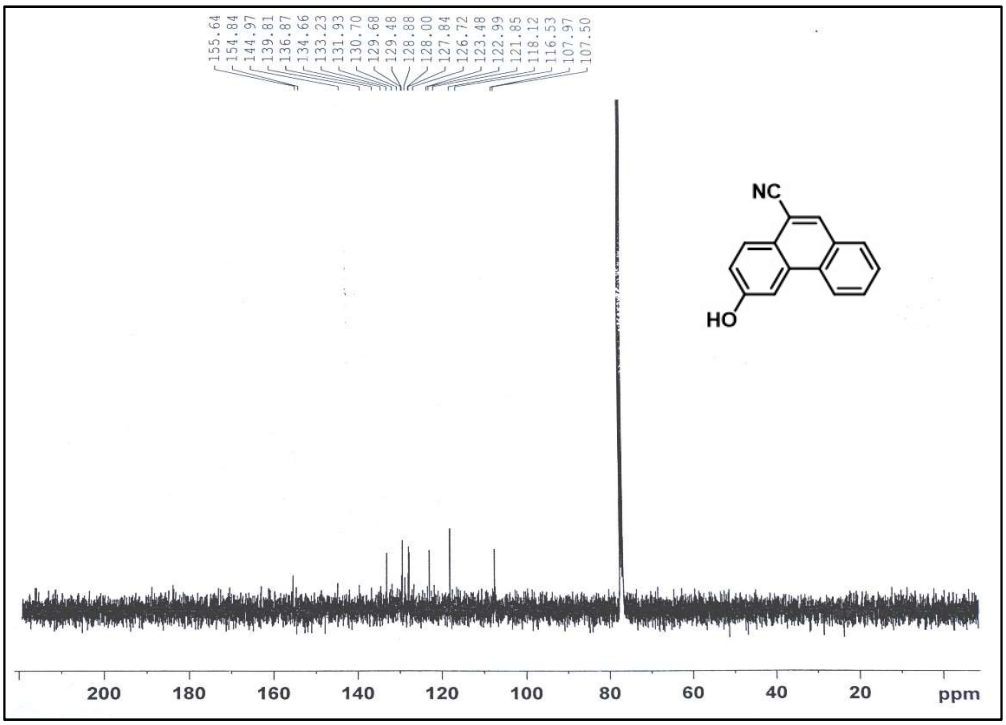

^{13}C NMR Spectrum of 55 ($CDCl_3$, 100 MHz)

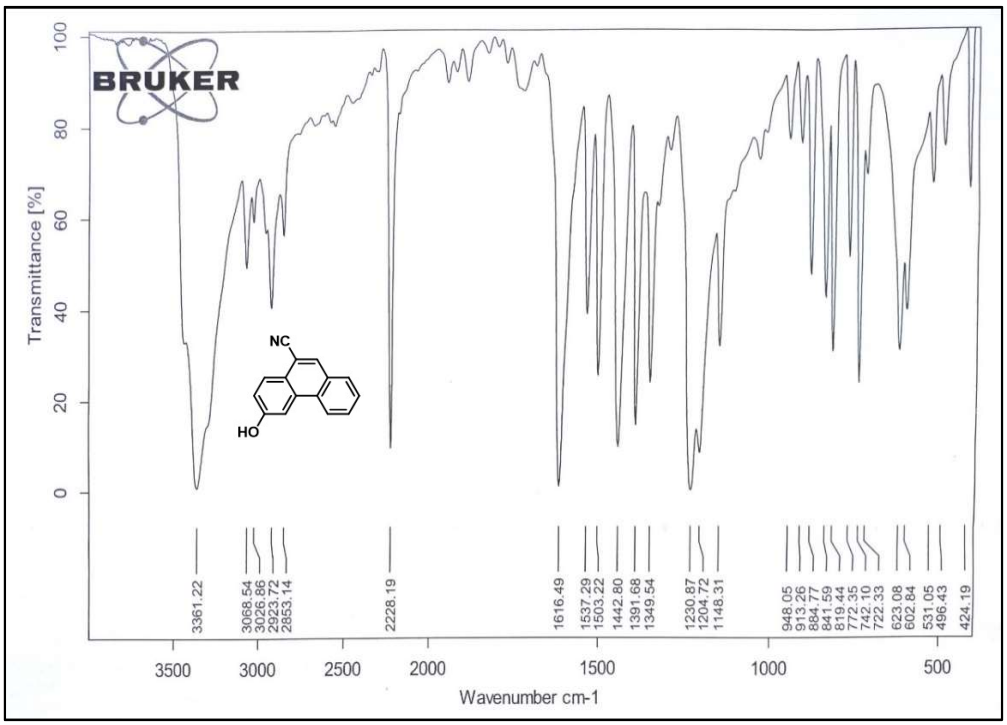

IR Spectrum of 55

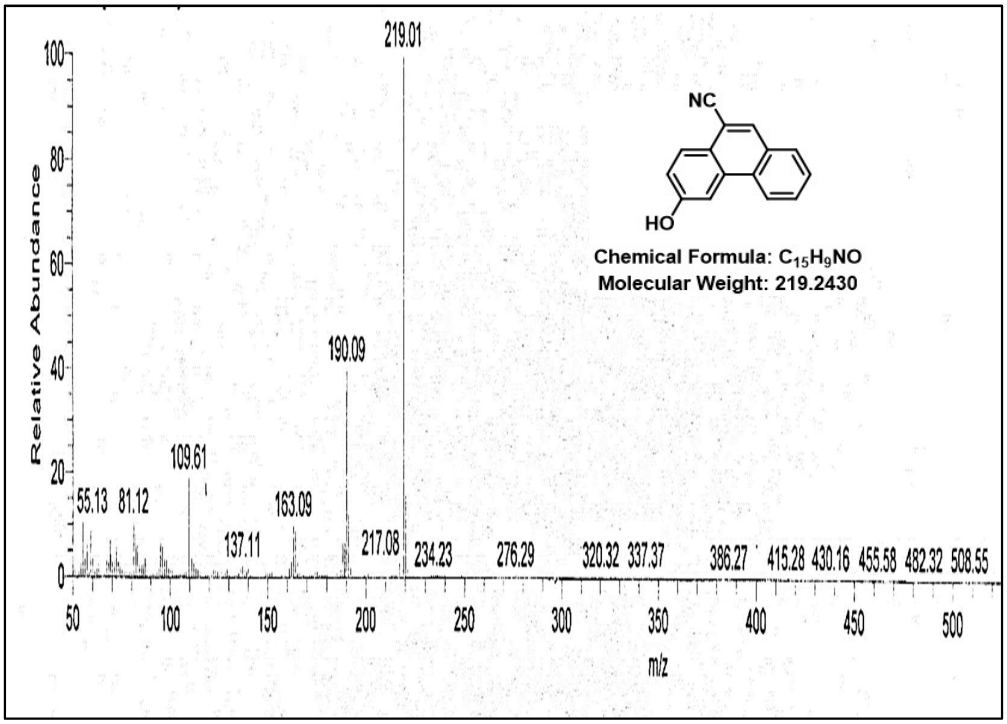

Mass Spectrum of 55

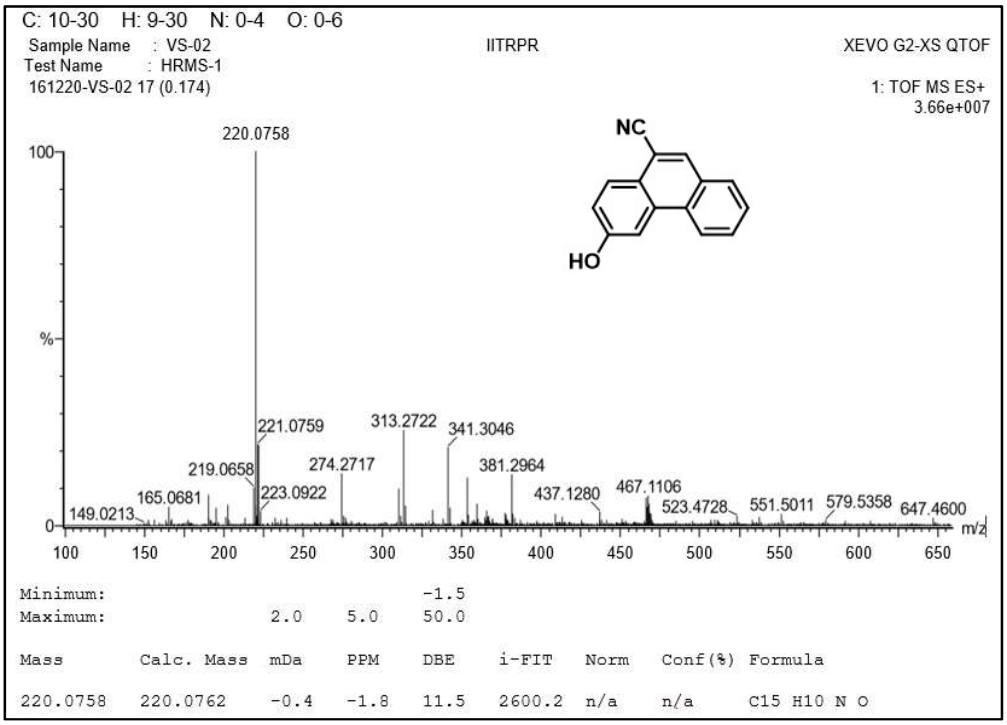

HRMS Spectrum of 55

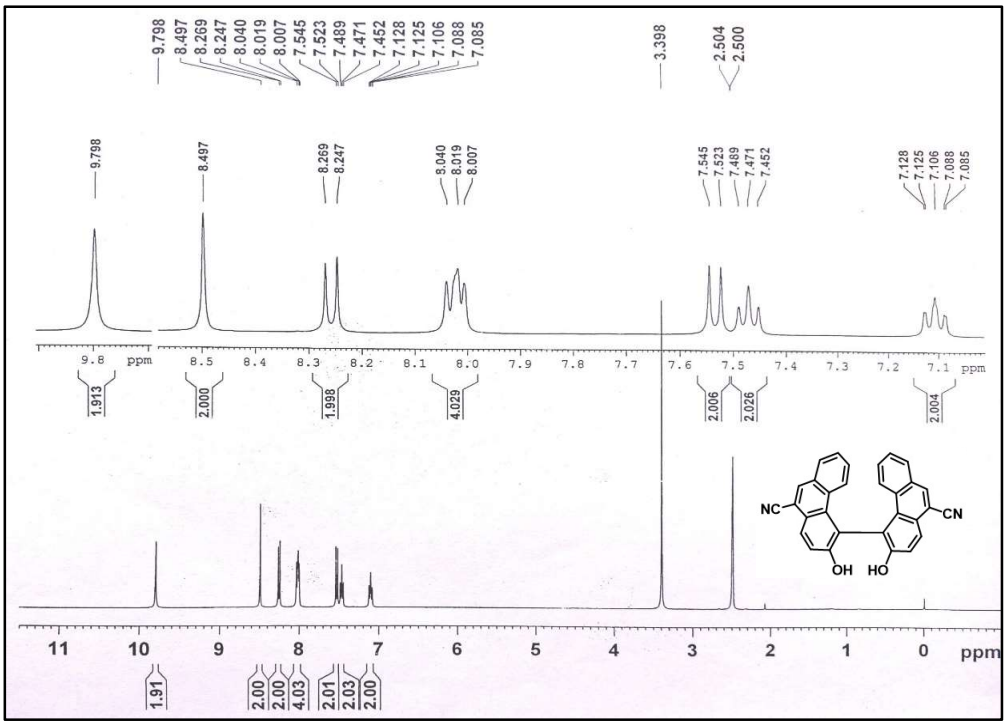

^{1}H NMR Spectrum of 56 (DMSO-d^{6}, 400 MHz)

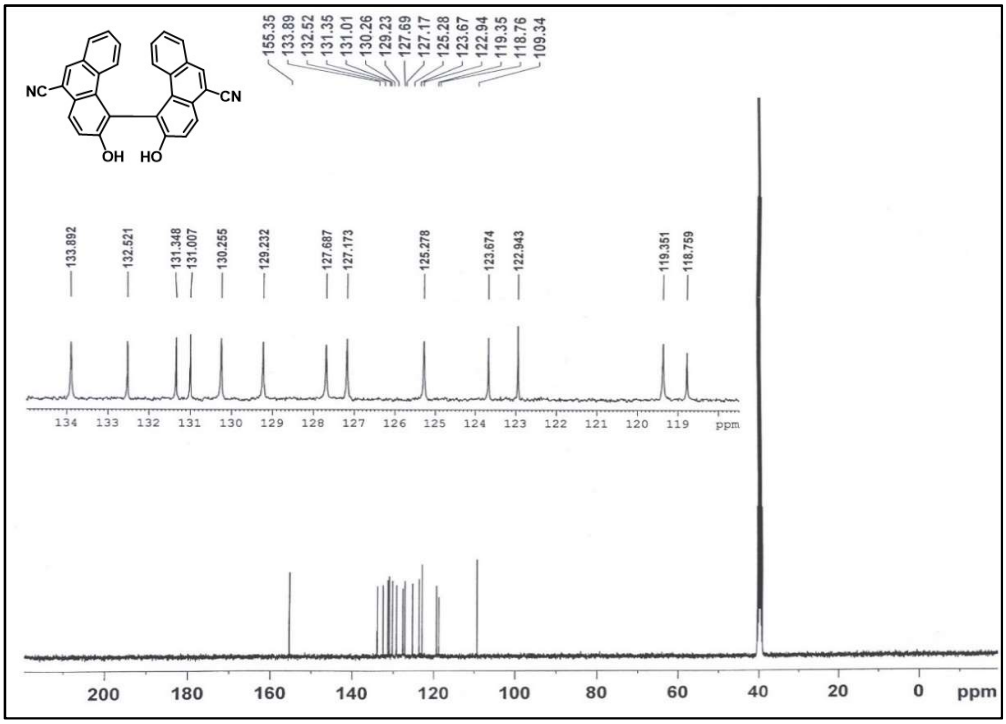

^{13}C NMR Spectrum of 56 (DMSO-d^6, 100 MHz)

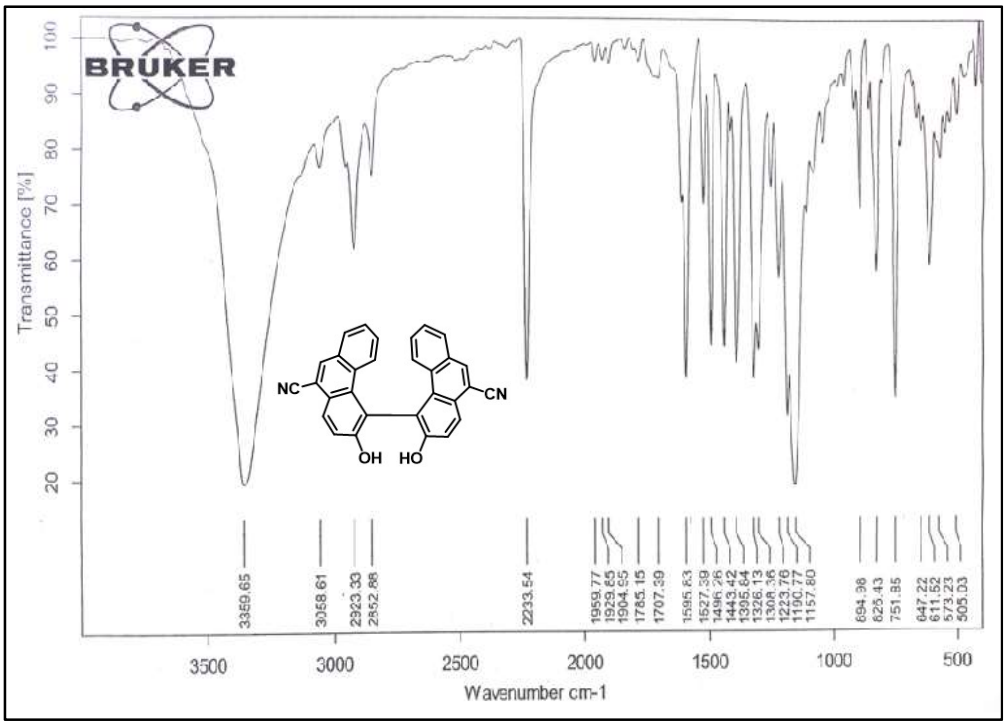

IR Spectrum of 56

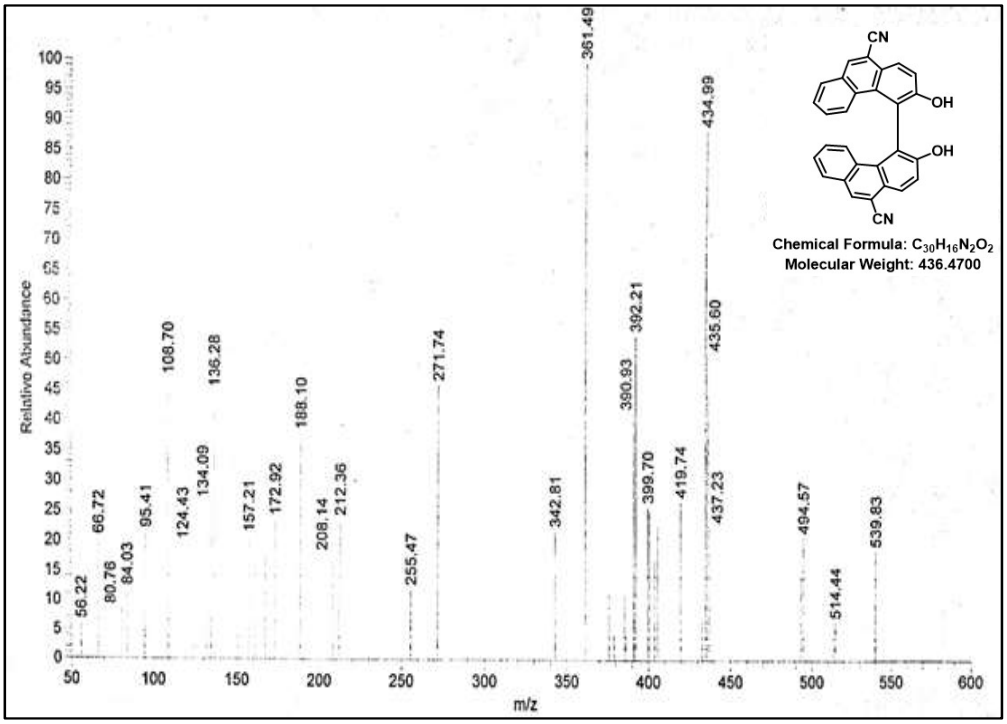

Mass Spectrum of 56

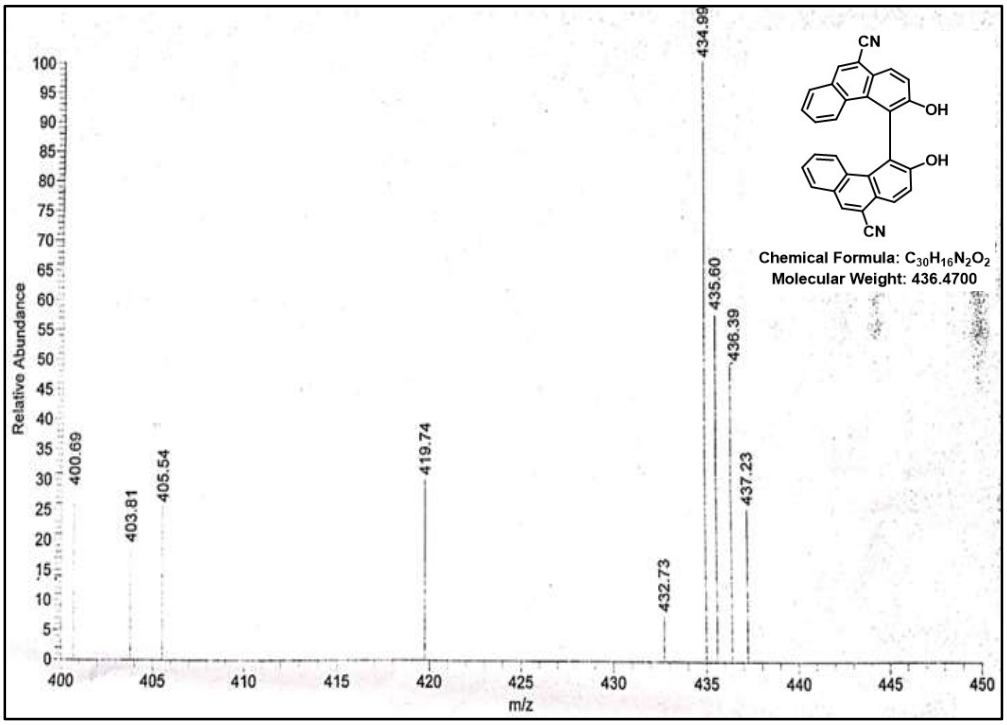

Expanded Mass Spectrum of 56

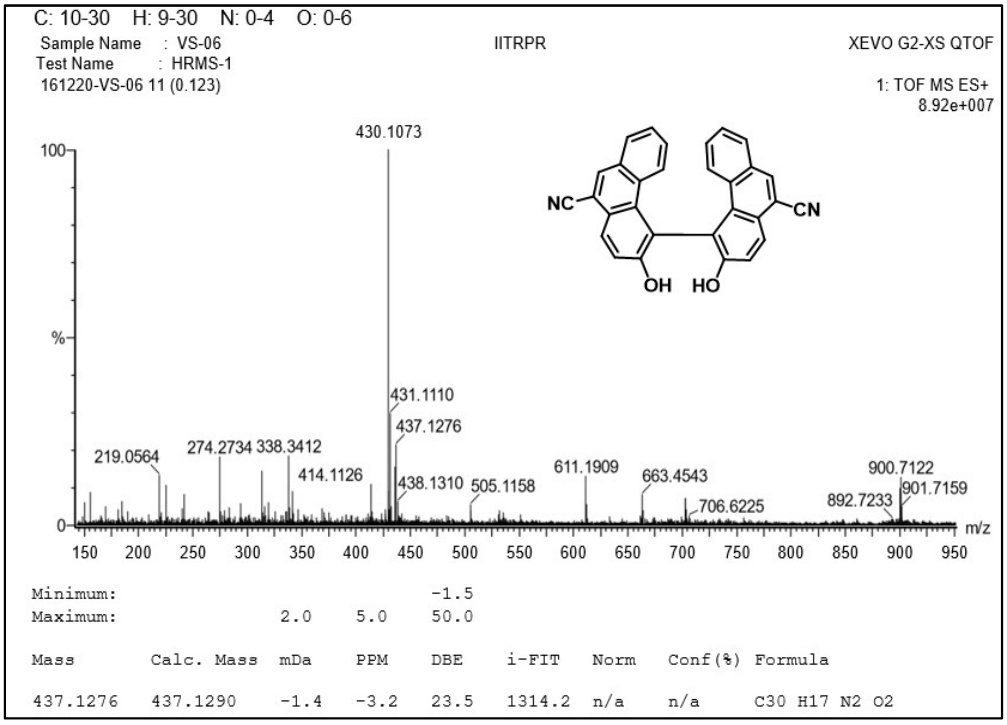

HRMS Spectrum of 56

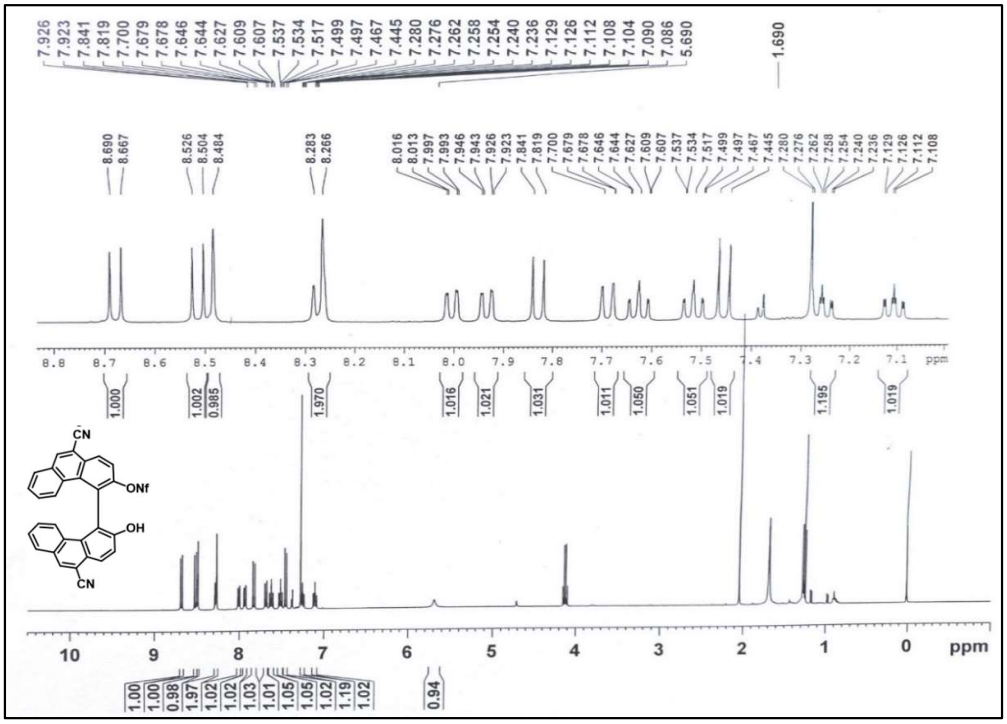

^{1}H NMR Spectrum of 57 ($CDCl_3$, 400 MHz)

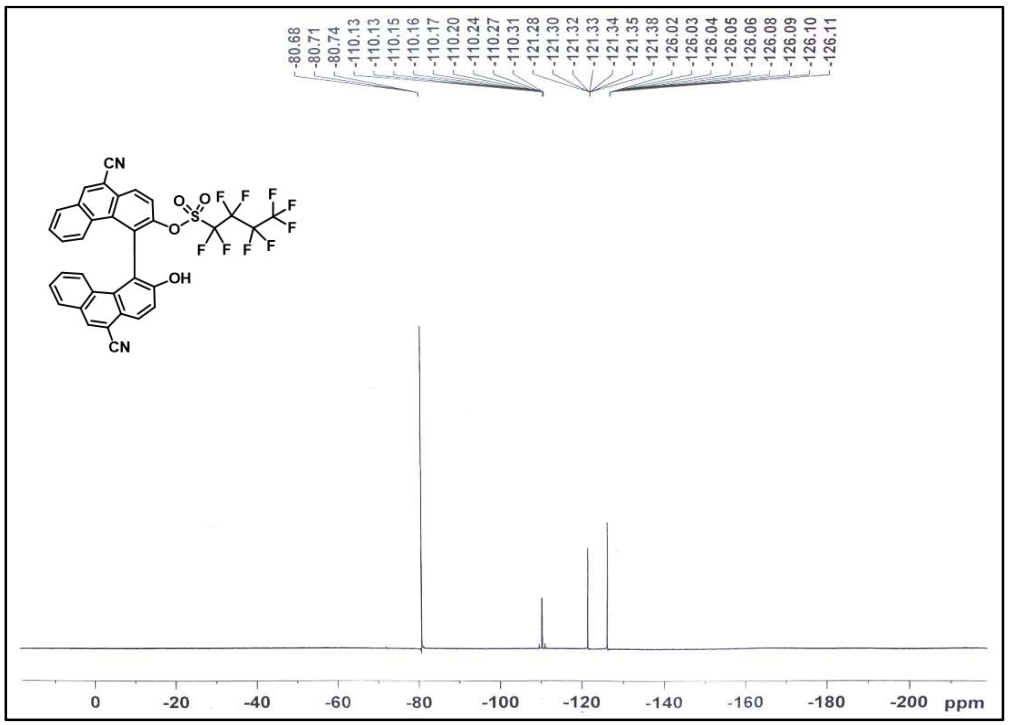

^{19}F NMR Spectrum of 57 ($CDCl_3$, 100 MHz)

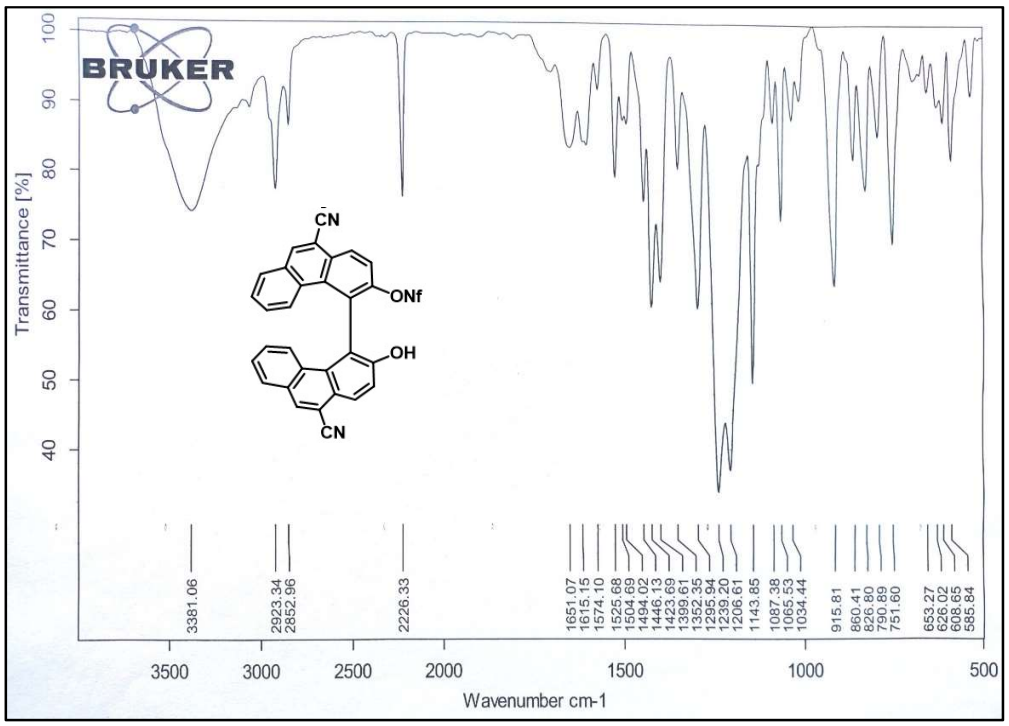

IR Spectrum of 57

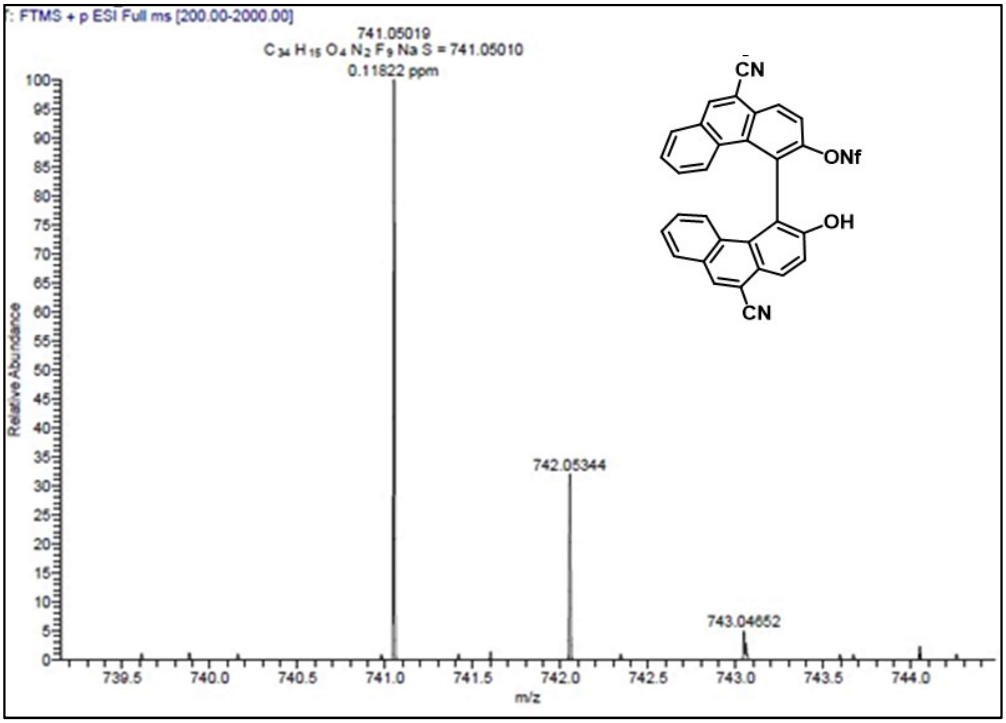

HRMS Spectrum of 57

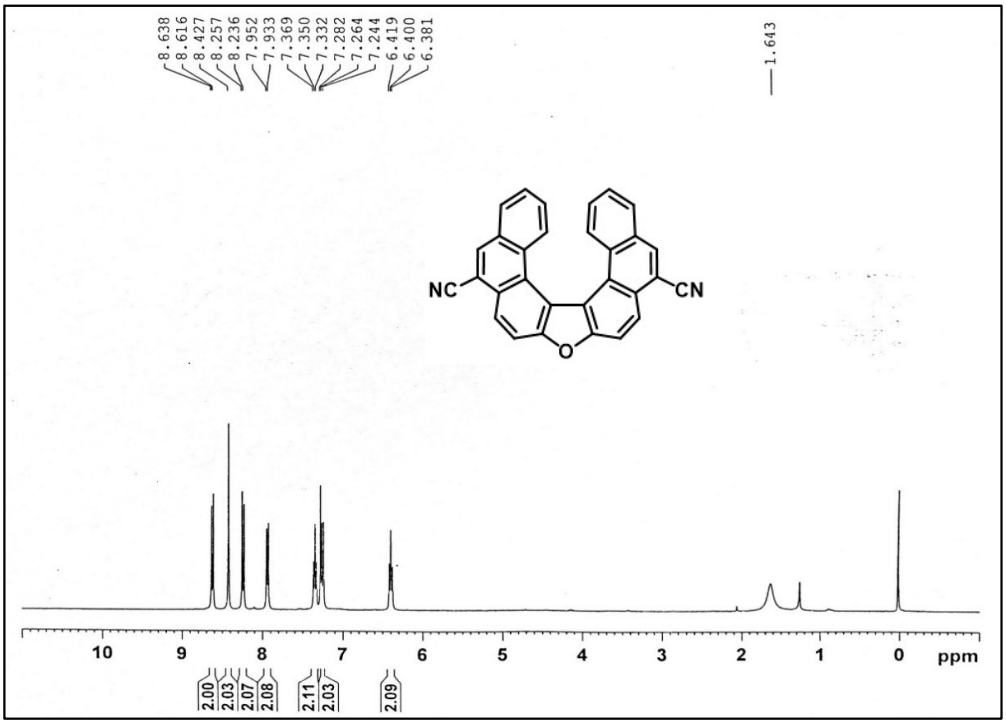

^{1}H NMR Spectrum of 50 ($CDCl_3$, 400 MHz)

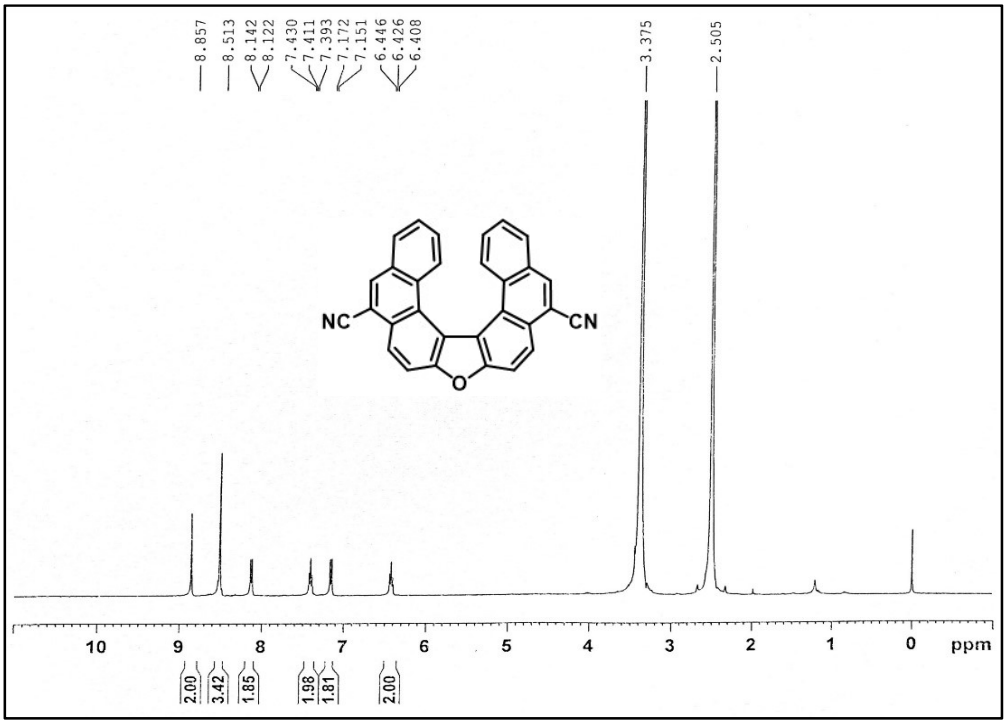

^{1}H NMR Spectra of 50 (DMSO-*d*^{6}, 400 MHz)

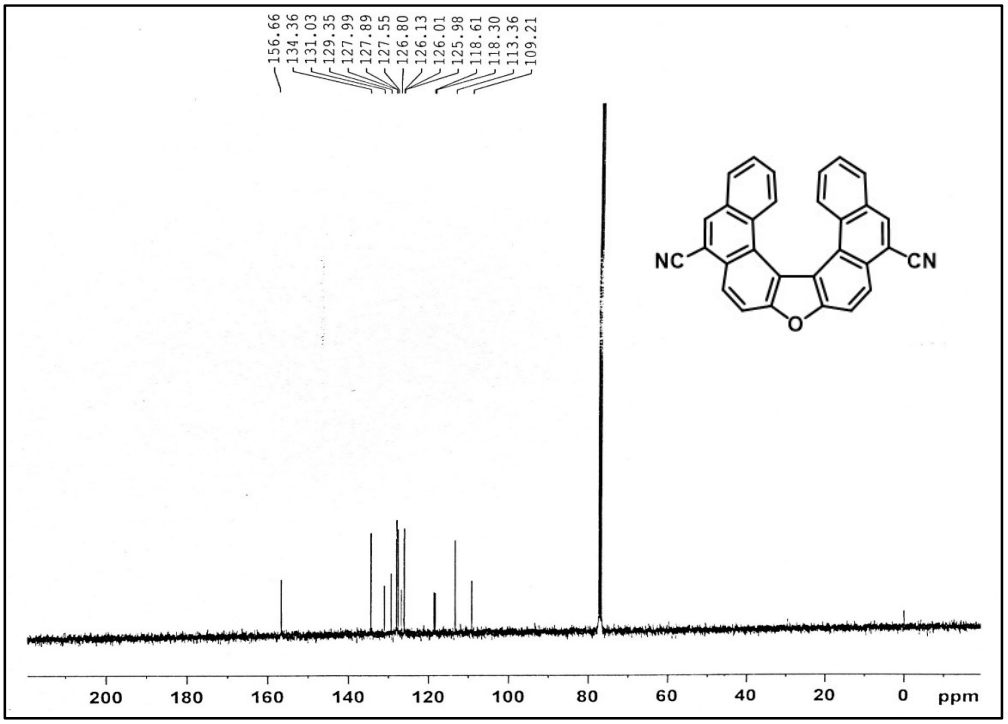

^{13}C NMR Spectrum of 50 ($CDCl_3$, 100 MHz)

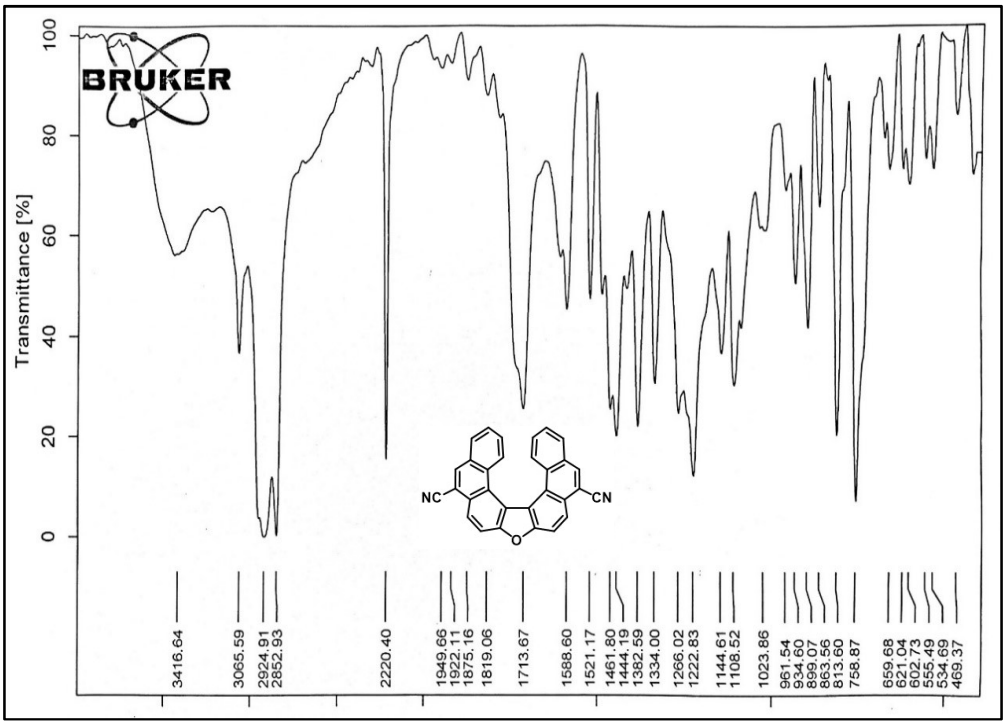

IR Spectrum of 50

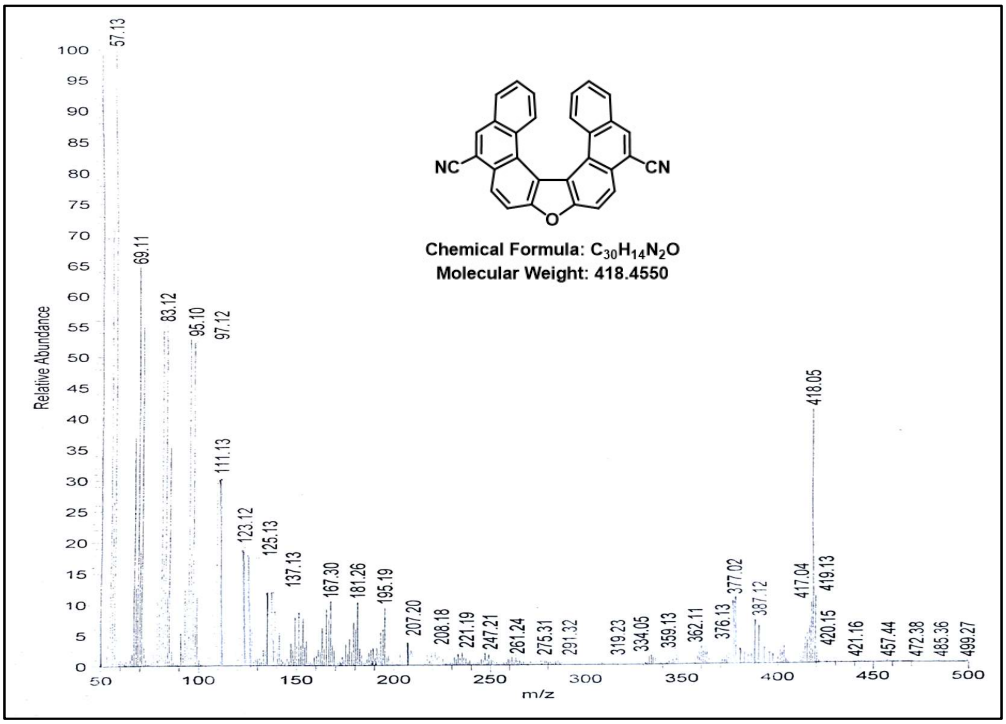

Mass Spectrum of 50

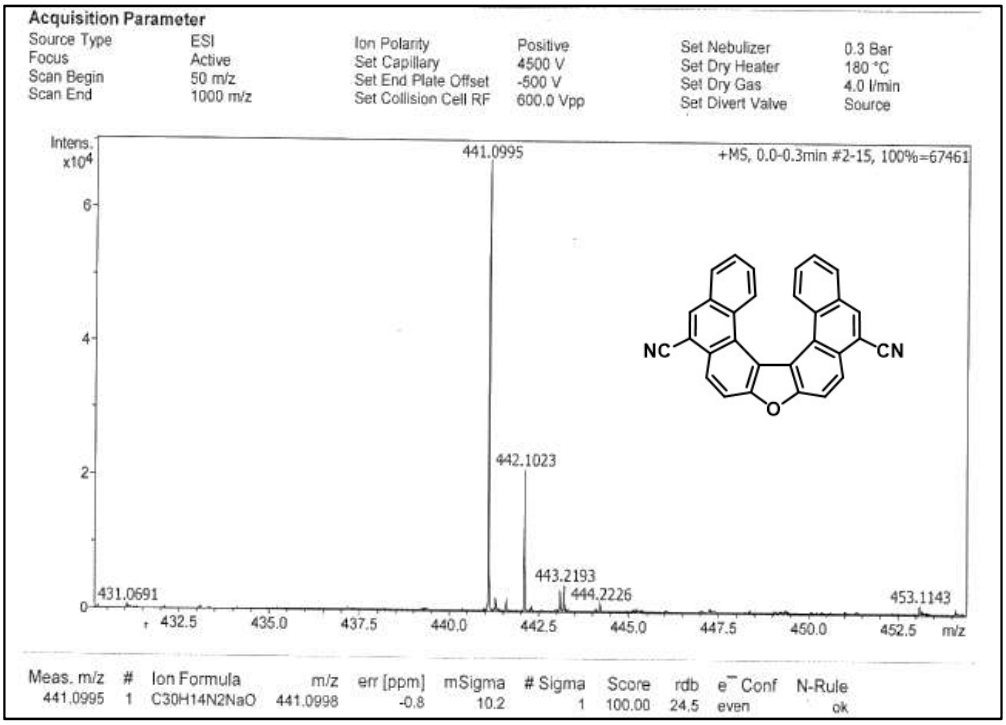

HRMS Spectrum of 50

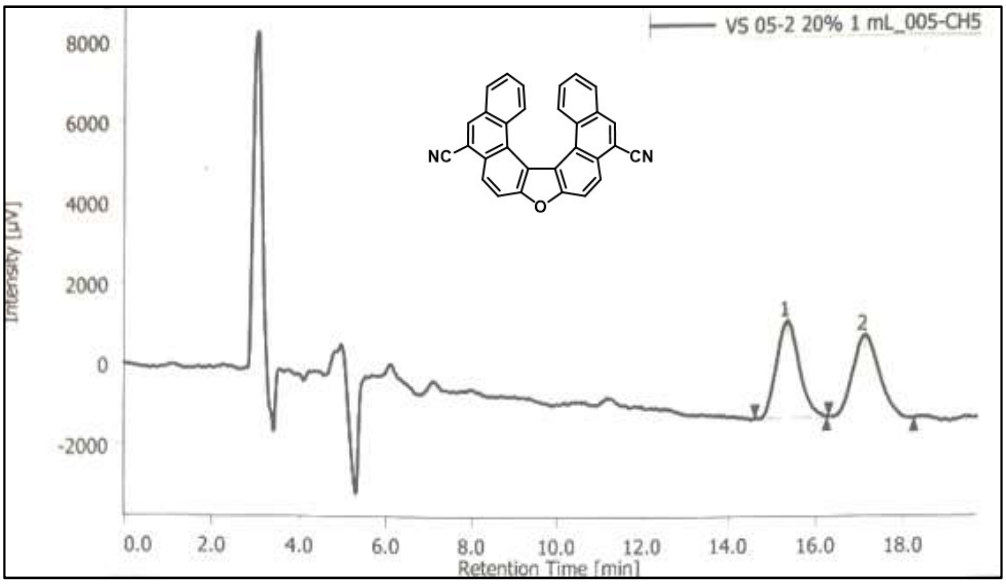

Peak Information

#	Peak Name	CH	tR [min]	Area [µV·sec]	Height [µV]	Area%	Height%	Quantity	NTP	Resolution	Symmetry Factor	Warning
1	Unknown	5	15.293	87190	2424	50.701	54.288	N/A	4166	1.738	1.205	
2	Unknown	5	17.070	84777	2041	49.299	45.712	N/A	3834	N/A	1.185	

HPLC Chromatogram of a single crystal of 50 obtained in toluene

3.7 Crystallographic Data

	50
Empirical formula	$C_{30}H_{14}N_2O$
Formula weight	418.43
Temperature/K	105(2) K
Wavelength	0.71073 Å
Crystal system	Monoclinic
Space group	P 21/n
a/Å	7.3131(2)
b/Å	16.1333(7)
c/Å	33.4675(15)
α/°	90
β/°	92.761(2)
γ/°	90
Volume/Å^3	3944.1(3) Å^3
Z	8
ρ_{calc}g/cm^3	1.409
μ/mm^{-1}	0.086
F(000)	1728
2Θ range for data collection/°	2.221 to 30.510°
Index ranges	-7<=h<=10, -23<=k<=20, -47<=l<=47
Reflections collected	36149
Independent reflections	11813 [R_{int} = 0.0661]
Data/restraints/parameters	11813 / 0 / 595
Goodness-of-fit on F^2	1.009
Final R indexes [I>=2σ (I)]	R_1 = 0.0862, wR_2 = 0.2027
Final R indexes [all data]	R_1 = 0.1170, wR_2 = 0.2262
Largest diff. peak/hole / e Å^{-3}	0.597 and -0.588 e.Å^{-3}

3.8 Computational Data

All DFT calculations were performed using Gaussian 09 Software. The ground state geometries of the helicene **50** was optimized by using the B3LYP functional. The B3LYP functional is a combination of Becke's three-parameter hybrid exchange functional4 and the Lee-Yang-Parr5 correlation functional. Basis set 6-31G was employed for the calculation. The results of the optimized geometry involving bond lengths, bond angles, intramolecular pitch of helicene were in close agreement to the results obtained from the X-ray crystallography data. The highest occupied molecular orbital (HOMO) – lowest occupied molecular orbital (LUMO) gap calculated using the B3LYP/6-31G level of theory for compound 4 was obtained to be 3.88 eV. The HOMO and LUMO energy levels were calculated to be -6.13 and -2.25 eV, respectively. Using the same level of calculations for helicene **48**, the HOMO and LUMO energy levels were calculated to be -6.17 and -2.19 eV, respectively. Thus, the HOMO-LUMO gap was found to be 3.98 eV for helicene **48**.

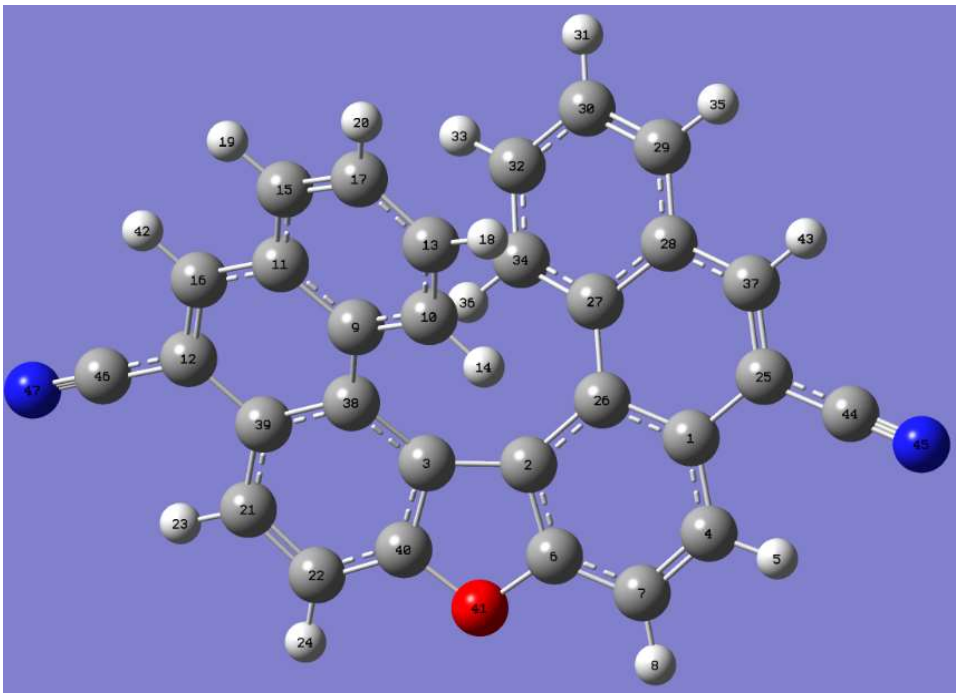

Optimized geometry with numbering

Cartesian co-ordinates of compound 50

Atom Numbers	Coordinates (Å) X	Y	Z
C1	3.131276	-0.962191	0.105105
C2	0.739228	-1.459315	-0.020484
C3	-0.739273	-1.459304	0.020413
C4	3.404270	-2.336108	0.352601
H5	4.424037	-2.637202	0.562046
C6	1.109612	-2.815341	0.080442
C7	2.406475	-3.287980	0.274042
H8	2.599974	-4.347247	0.382947
C9	-1.647572	0.817214	0.784765
C10	-0.485618	1.212885	1.493636
C11	-2.743150	1.739002	0.739502
C12	-4.214470	0.005064	-0.133805
C13	-0.375255	2.477586	2.050739
H14	0.319978	0.505343	1.628278
C15	-2.593089	3.041318	1.281950
C16	-4.003716	1.315384	0.222579
C17	-1.423339	3.413186	1.920283
H18	0.523690	2.746575	2.595250
H19	-3.428860	3.731555	1.216174
H20	-1.321828	4.406553	2.344160
C21	-3.404343	-2.336052	-0.352598
C22	-2.406558	-3.287940	-0.274085
H23	-4.424122	-2.637130	-0.562008
H24	-2.600077	-4.347203	-0.382990
C25	4.214439	0.004998	0.133885
C26	1.804771	-0.510123	-0.205955
C27	1.647597	0.817198	-0.784800
C28	2.743188	1.738970	-0.739467
C29	2.593180	3.041293	-1.281912

C30	1.423477	3.413184	-1.920317
H31	1.322007	4.406554	-2.344194
C32	0.375392	2.477596	-2.050855
H33	-0.523510	2.746599	-2.595430
C34	0.485701	1.212889	-1.493755
H35	3.428957	3.731517	-1.216078
H36	-0.319888	0.505356	-1.628472
C37	4.003720	1.315327	-0.222485
C38	-1.804796	-0.510097	0.205917
C39	-3.131320	-0.962142	-0.105093
C40	-1.109683	-2.815323	-0.080510
O41	-0.000041	-3.654826	-0.000045
H42	-4.819975	2.028339	0.175492
H43	4.819988	2.028269	-0.175348
C44	5.521412	-0.409143	0.542580
N45	6.593234	-0.751998	0.880584
C46	-5.521470	-0.409051	-0.542444
N47	-6.593313	-0.751885	-0.880402

3.9 References

1. (a) Bunz, U. H. F. α-Oligofurans: Molecules without a Twist, *Angew. Chem. Int. Ed*. **2010**, *49*, 5037. (b) Horner, K. E.; Karadakov, P. B. Chemical Bonding and Aromaticity in Furan, Pyrrole, and Thiophene: A Magnetic Shielding Study, *J. Org. Chem*. **2013**, *78*, 8037.
2. (a) Tsuji, H.; Mitsui, C.; Ilies, L.; Sato, Y.; Nakamura, E. Synthesis and Properties of 2,3,6,7-Tetraarylbenzo[1,2-*b*:4,5-*b*′]difurans as Hole-Transporting Material, *J. Am. Chem. Soc*. **2007**, *129*, 11902. (b) Mitsui, C.; Soeda, J.; Miwa, K.; Tsuji, H.; Takeya, J.; Nakamura, E. Naphtho[2,1-*b*:6,5-*b*']difuran: a Versatile Motif Available for Solution-processed Single-crystal Organic Field-effect Transistors with High Hole Mobility, *J. Am. Chem. Soc*. **2012**, *134*, 5448. (c) Nakano, M.; Niimi, K.; Miyazaki, E.; Osaka, I.; Takimiya, K. Isomerically Pure Anthra[2,3-*b*:6,7-*b*′]-difuran (anti-ADF), -dithiophene (*anti*-ADT), and -diselenophene (*anti*-ADS): Selective Synthesis, Electronic Structures, and Application to Organic Field-Effect Transistors, *J. Org. Chem*. **2012**, *77*, 8099.
3. Cui, Y.; Ngo, H. L.; Lin, W.; Hill, C.; Carolina, N. New Rigid Angular Dicarboxylic Acid for the Construction of Nanoscopic Supramolecules: From a Molecular Rectangle to a 1-D Coordination Polymer, *Inorg. Chem*. **2002**, *41*, 1033.
4. Areephong, J.; Ruangsupapichart, N.; Thongpanchang, T. A concise synthesis of functionalized 7-oxa-[5]-helicenes, *Tetrahedron Lett*. **2004**, *45*, 3067.
5. Schneider, J. F.; Nieger, M.; Nättinen, K.; Dötz, K. H. A novel approach to functionalized heterohelicenes via chromium-templated benzannulation reactions, *Synthesis* **2005**, *7*, 1109.
6. Sundar, M. S.; Sahoo, S.; Bedekar, A. V. Synthesis and study of the structural properties of oxa[5]helicene derivatives, *Tetrahedron: Asymmetry* **2016**, *27*, 777.
7. Eskildsen, J.; Krebs, F. C.; Sommer-larsen, P.; Bechgaard, K. Preparation and Structural Properties of 7,8-Dioxa[6]helicenes and 7a,14c-Dihydro-7,8-dioxa[6]helicenes, *J. Org. Chem*. **2001**, *66*, 200.
8. (a) Hasan, M.; Pandey, A. D.; Khose, V. N.; Mirgane, N. A.; Karnik, A. V. Sterically Congested Chiral 7,8-Dioxa[6]helicene and Its Dihydro Analogues: Synthesis, Regioselective Functionalization, and Unexpected Domino Prins Reaction, *Eur. J. Org. Chem.* **2015**, 3702. (b) Hasan, M.; Khose, V. N.; Mori, T.; Borovkov, V.; Karnik, A. V. Sui Generis Helicene-Based Supramolecular Chirogenic System: Enantioselective Sensing, Solvent Control, and Application in Chiral Group Transfer Reaction, *ACS*

Omega **2017**, *2*, 592.

9. Hasan, M.; Khose, V. N.; Pandey, A. D.; Borovkov, V.; Karnik, A. V. Tailor-Made Supramolecular Chirogenic System Based on Cs-Symmetric Rigid Organophosphoric Acid Host and Amino Alcohols: Mechanistic Studies, Bulkiness Effect, and Chirality Sensing, *Org. Lett*. **2016**, *18*, 440.
10. Liu, P.; Bao, X.; Naubron, J.–V.; Chentouf, S.; Humbel, S.; Vanthuyne, N.; Jean, M.; Giordano, L.; Rodriguez, J.; Bonne D. Simultaneous Control of Central and Helical Chiralities: Expedient Helicoselective Synthesis of Dioxa[6]helicenes, *J. Am. Chem. Soc*. **2020**, *142*, 16199.
11. Ryo, I.; Akihiro, T.; Suguru, U.; Tatsushi, I.; Kazunobu, I.; Taisuke, M.; Katsuhiko, T.; Shinsuke, K.; Tatsuya, U.; Tsutomu, K. Synthesis and Stereochemical Behavior of a New Chiral Oxa[7]heterohelicene, *Chem. Lett.* **2011**, *40*, 1343.
12. Nakano, K.; Hidehira, Y.; Takahashi, K.; Hiyama, T.; Nozaki, K. Stereospecific Synthesis of Hetero[7]helicenes by Pd-Catalyzed Double N-Arylation and Intramolecular O-Arylation, *Angew. Chemie - Int. Ed*. **2005**, *44*, 7136.
13. (a) Salim, M.; Akutsu, A.; Kimura, T.; Minabe, M.; Karikomi, M. Novel synthesis of oxa[9]helicenes by Lawesson's reagent-mediated cyclization of helical quinone derivatives, *Tetrahedron Lett*. **2011**, *52*, 4518. (b) Shahabuddin, M.; Ohgoshi, K.; Hossain, M. S.; Kimura, T.; Karikomi, M. Synthesis of helical shaped 1,1′-bibenzo[c]phenanthrene-2,2′-diol (HEBPOL) derivatives by reduction of helical quinones, *Tetrahedron Lett*. **2017**, *58*, 3704. (c) Salim, M.; Ubukata, H.; Kimura, T.; Karikomi, M. Novel synthesis of alkoxy substituted oxa[9]helicenes by the reaction of helical quinone with alcohols, *Tetrahedron Lett.* **2011**, *52*, 6591.
14. Miah, J.; Shahabuddin, M.; Kayes, N.; Karikomi, M.; Nasuno, E.; Kato, N.; Iimura, K. Fabrication and Characterization of Molecular Films of 11-Oxa[9]helicene and 9-Diethyleneglycoxy-11-oxa[9]helicene, *Trans. Mat. Res. Soc. Japan* **2016**, *41*, 151.
15. Sundar, M. S.; Bedekar, A. V. Synthesis and Study of 7,12,17-Trioxa[11]helicene, *Org. Chem.* **2015**, *17*, 5808.
16. Yanagi, T.; Tanaka, T.; Yorimitsu, H. Asymmetric systematic synthesis, structures, and (chir)optical properties of a series of dihetero[8] helicenes, *Chem. Sci*. **2021**, *12*, 2784.
17. Wachsmann, C.; Weber, E.; Czugler, M.; Seichter, W. New Functional Hexahelicenes − Synthesis, Chiroptical Properties, X-ray Crystal Structures, and Comparative Data Bank Analysis of Hexahelicenes, *Eur. J. Org. Chem*. **2003**, 2863.
18. Stçhr, M.; Boz, S.; Schar M.; Nguyen, M. T.; Pignedoli, C. A.; Passerone, D.;

Schweizer, W. B.; Thilgen, C.; Jung, T. A. Diederich, F. Self-Assembly and Two-Dimensional Spontaneous Resolution of Cyano-Functionalized [7]Helicenes on Cu(111), *Angew. Chem. Int.Ed*. **2011**, *50*, 9982.

19. Upadhyay, G. M.; Mande, H. M.; Pithadia, D. K.; Maradiya, R. H.; Bedekar, A. V. Effect of the Position of the Cyano Group on Molecular Recognition, Supramolecular Superhelix Architecture, and Spontaneous Resolution of Aza[7]helicenes, *Cryst. Growth Des*. **2019**, *19*, 5354.
20. Gupta, R.; Cabreros, T.A.; Muller, G.; Bedekar, A.V. Synthesis and study of enantiomerically pure 5,13-dicyano-9-oxa[7]helicene, *Eur. J. Org. Chem.* **2018**, 5397.
21. Talele, H. R.; Chaudhary, A. R.; Patel, P. R. Expeditious synthesis of helicenes using an improved protocol of photocyclodehydrogenation of stilbenes, *ARKIVOC* **2011**, *9*, 15.
22. McOmie, J. F. W.; Watts, M. L.; West, D. E. Demethylation of aryl methyl ethers by boron tribromide, *Tetrahedron* **1968**, *24*, 2289.
23. Raouafi, S.; Aloui, F. Synthesis and photophysical properties of new nitrile grafted benzo[ghi]perylene derivatives, *J. Mol. Struct*. **2019**, *1195*, 153.
24. Negi, A. S.; Chattopadhyay, S. K.; Srivastava, S.; Bhattacharya, A. K. A Simple Regioselective Demethylation of p Aryl Methyl Ethers Using Aluminum Chloride Dichloromethane System, *Synth. Commun*. **2005**, *35*, 15.
25. Toda, F.; Tanaka, K.; Iwata, S. Oxidative coupling reactions of phenols with iron(III) chloride in the solid state, *J. Org. Chem*. **1989**, *54*, 3007.
26. Yamamoto, K.; Fukushima, H.; Okamoto, Y.; Hatada, K.; Nakazaki, M. Synthesis and chiral recognition of optically active crown ethers incorporating a biphenanthryl moiety as the chiral centre, *Chem. Commun.* **1984**, 1111.
27. Smrcina, M.; Polakova, J.; Vyskocil, S.; Kocovsky, P. Synthesis of enantiomerically pure binaphthyl derivatives. Mechanism of the enantioselective, oxidative coupling of naphthols and designing a catalytic cycle, *J. Org. Chem.* **1993**, *58*, 4534.
28. Noji, M.; Nakajima, M.; Koga, K. A new catalytic system for aerobic oxidative coupling of 2-naphthol derivatives by the use of CuCl-amine complex: A practical synthesis of binaphthol derivatives, *Tetrahedron Lett.* **1994**, *35*, 7983.
29. Takizawa, S.; Kodera, J.; Yoshida, Y.; Sako, M.; Breukers, S.; Enders, D.; Sasai, H. Enantioselective oxidative-coupling of polycyclic phenols, *Tetrahedron* **2014**, *70*, 1786.
30. Terrasson, V.; Roy, M.; Moutard, S.; Lafontaine, M. –P.; Pèpe, G.; Félix, G.; Gingras, M. Benzylic-type couplings provide an important asymmetric entry to functionalized, non-racemic helicenes, *RSC Adv.* **2014**, *4*, 32412.

31. Nakano, K.; Hidehira, Y.; Takahashi, K.; Hiyama, T.; Nozaki, K. Stereospecific Synthesis of Hetero[7]helicenes by Pd-Catalyzed Double N-Arylation and Intramolecular O-Arylation, *Angew. Chem. Int. Ed*. **2005**, *44*, 7136.
32. Upadhyay, G. M.; Talele, H. R.; Sahoo, S.; Bedekar, A. V. Synthesis of carbazole derived aza[7]helicenes, *Tetrahedron Lett*. **2014**, *55*, 5394.
33. Murayama, K.; Oike, Y.; Furumi, S.; Takeuchi, M.; Noguchi, K.; Tanaka, K. Enantioselective Synthesis, Crystal Structure, and Photophysical Properties of a 1,1′-Bitriphenylene-Based Sila[7]helicene, *Eur. J. Org. Chem*. **2015**, *2015*, 1409.
34. Virk, T. S.; Ilawe, N. V.; Zhang, G.; Yu, C. P.; Wong, B. M. Sultam-Based Hetero[5]helicene: Synthesis, Structure, and Crystallization-Induced Emission Enhancement, *ACS Omega* **2016**, *1*, 1336.
35. Caldwell, R. A.; Ghali, N. I.; Chein, C. K.; DeMarco, D.; Smith L. Photocycloaddition of beta-methylstyrenes to some 9-cyanophenanthrenes. Chemical Consequences of exciplex formation, *J. Am. Chem. Soc*. **1978**, *100*, 2857.